JACS
JOURNAL OF THE AMERICAN CHEMICAL SOCIETY

ARTICLE

pubs.acs.org/JACS

Regioselectivity of H Cluster Oxidation

Marta K. Bruska, Martin T. Stiebritz, and Markus Reiher*

Laboratorium für Physikalische Chemie, ETH Zurich, Wolfgang-Pauli-Strasse 10 8093 Zürich, Switzerland

Supporting Information

ABSTRACT: The H_2-evolving potential of [FeFe] hydrogenases is severely limited by the oxygen sensitivity of this class of enzymes. Recent experimental studies on hydrogenase from *C. reinhardtii* point to O_2-induced structural changes in the $[Fe_4S_4]$ subsite of the H cluster. Here, we investigate the mechanistic basis of this observation by means of density functional theory. Unexpectedly, we find that the isolated H cluster shows a pathological catalytic activity for the formation of reactive oxygen species such as O_2^- and HO_2^-. After protonation of O_2^-, an OOH radical may coordinate to the Fe atoms of the cubane, whereas H_2O_2 specifically reacts with the S atoms of the cubane-coordinating cysteine residues. Both pathways are accompanied by significant structural distortions that compromise cluster integrity and thus catalytic activity. These results explain the experimental observation that O_2-induced inhibition is accompanied by distortions of the $[Fe_4S_4]$ moiety and account for the irreversibility of this process.

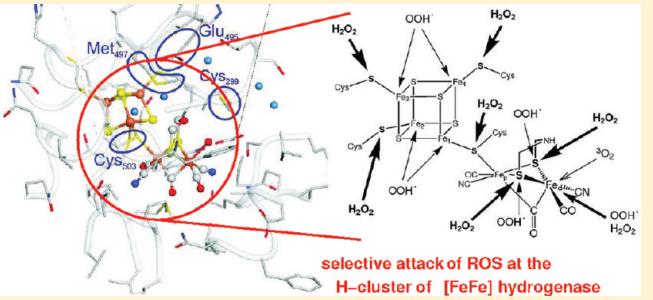

1. INTRODUCTION

Hydrogenases are enzymes capable of catalyzing the reversible oxidation of hydrogen[1−7] and have therefore attained attention in the field of clean energy research.[8−10] However, a generally high sensitivity to molecular oxygen complicates their technological application.

Hydrogenases are classified into three different groups according to phylogenetic relations and composition of their active sites. There exist [FeFe], [NiFe], and [Fe] hydrogenases, which vary in their catalytic activity as well as in their sensitivity against dioxygen.

[Fe] hydrogenase is the only air-stable form, but oxygen-tolerant [NiFe] hydrogenases have also been discovered (see below). In its catalytic mechanism [Fe] hydrogenase differs substantially from [NiFe] and [FeFe] hydrogenases, as the cofactor methylenetetrahydromethanopoterin acts as a hydride acceptor following heterolytic cleavage ozf H_2.[11,12] Oxygen-induced inhibition is best understood for [NiFe] hydrogenases and involves two states. The less oxidized Ni−B state is readily reactivated upon reduction by one electron and, according to X-ray data, harbors a hydroxy ligand that bridges the Ni and the Fe center of the active site. In the unready Ni−A state, which is hard to reactivate, the same position is probably occupied by a hydroperoxo species.[13]

Interestingly, apart from enzyme variants with amino acid substitutions in the gas diffusion channel,[14,15] remarkably oxygen tolerant [NiFe] hydrogenase variants were identified in *R. eutropha* and *A. aeolicus*.[16−19] Analysis of the membrane-bound hydrogenase of *R. eutropha* revealed the presence of six instead of the usual four cysteine residues in the vicinity of the H clusters cubane moiety which are crucial for the increased O_2 tolerance of this enzyme.[18] These variants provide the first direct link between changes in the primary sequence of the protein and altered reactivity of the active site with respect to O_2. However, a mechanistic explanation for this observation and evidence that this structural feature can be transferred to other hydrogenases are still lacking.

In terms of hydrogen formation, [FeFe] hydrogenases show the highest catalytic activity and are therefore the most interesting candidates for clean energy production. At the same time, however, they are most sensitive to molecular oxygen. O_2-tolerant [FeFe] hydrogenases have not yet been identified or designed, and oxygen exposition of the active enzyme even at low oxygen levels rapidly leads to irreversible inactivation accompanied by the loss of H cluster signals in electron paramagnetic resonance (EPR) spectroscopy.[20,21] Interestingly, species-dependent differences in O_2 sensitivity exist[22] which point to the possibility of obtaining enzyme variants with increased O_2 tolerance by means of protein engineering. A prerequisite for this undertaking is to understand the mechanism of O_2-induced inhibition which up to now has not been unambiguously elucidated.

In a theoretical study we addressed this question and showed that O_2 exothermically coordinates to the distal Fe_d atom of the H cluster,[23] which is in line with experimental findings obtained by protein film voltammetry.[22] Protonation and water abstraction can lead to a highly reactive oxo compound that could further react by disintegrating the ligand environment of the $2[Fe]_H$ subsite.[23] Dioxygen coordination to the H cluster was also studied in a quantum mechanics/molecular mechanics

Received: September 29, 2011
Published: November 22, 2011

dx.doi.org/10.1021/ja209165r | *J. Am. Chem. Soc.* 2011, 133, 20588–20603

(QM/MM) approach by Dogaru et al.,[24] in which the QM region comprised only the 2[Fe]$_H$ subcluster but not the [Fe_4S_4] cubane which we find to be of crucial importance because of magnetic coupling subtleties within the H cluster. Of course, reactions that occur at the cubane subcluster also require a QM description.

Remarkably, O_2 binding is clearly determined by the precise ligand arrangement around the active Fe_d atom. We showed that the active site of [Fe] and [FeFe] hydrogenases share a common structural principle that allows one to relate both.[25] In sharp contrast to [FeFe] hydrogenase, coordination of O_2 to the active iron atom of [Fe] hydrogenase is endothermic[26,27] (also found by Dey[28]), which accounts for the oxygen tolerance of this enzyme. When we swap the first-shell ligand environment of the Fe_d atom into that of the central Fe atom of [Fe] hydrogenase, we obtain almost an inversion of the sign of the O_2 coordination energy: Fe_d binds O_2 less exothermically, whereas the binding to the Fe atom of [Fe] hydrogenase in a swapped ligand sphere becomes exothermic.[27]

Experimental studies on the [FeFe] hydrogenase from *C. reinhardtii* led to the suggestion that oxygen-induced inactivation is connected with dramatic structural changes in the cubane subsite of the H cluster caused by reactive oxygen species such as O_2^-.[29] Such a mechanism was shown to be crucial for the enzyme aconitase, where oxidation is supposed to induce release of a Fe^{2+} ion from the cubane in the active site to produce a [Fe_3S_4] cluster.[30] Because of the numerous sulfur-containing ligands surrounding the H cluster an alternative mechanism of oxygen-induced degradation consists of sulfoxygenation, as discussed in a recent review by Darensbourg and Weigand.[31]

Here, we employ density functional theory to investigate possible reaction pathways for the formation of reactive oxygen species and their subsequent attack at the cubane subsite of the H cluster (for details on the computational methodology see the Appendix, where we also discuss possible shortcomings of our approach). We focus on the isolated metal cluster (anchored by thiomethanolate ligands in positions as in the full protein) because a comprehensive analysis of its reactivity with respect to O_2 is the prerequisite to analyze and understand the influence of the protein environment in which it is embedded. Because of the huge multitude of possible reaction pathways determined by the specific attack sites at the H cluster, the type of the reactive oxygen species, and the overall charge and spin states as well as by the modulation of amino acid residues in the vicinity of the active site, a direct attempt to tackle the problem from the start with a full structural model of the protein is hardly feasible and may obstruct the discovery of the principles of the process, as the results would have been obtained only for a specific enzyme. In contrast, the present study of the generic active site will open up the path for protein engineering attempts to design a more oxygen-tolerant enzyme variant. Still, the elucidation of all possible oxidation pathways at the generic (anchored) H cluster is already a formidable task, as will become evident in the discussion to follow.

2. REACTIVITY OF O_2 ALONG THE H CLUSTER

While we have already studied oxygen-induced decomposition reactions at the distal iron atom in detail in refs 23, 27, and 32, we here consider a detachment of the O_2 ligand to facilitate its diffusion along the cluster toward the [Fe_4S_4] cubane. In our quantum chemical calculations we choose an H cluster model as

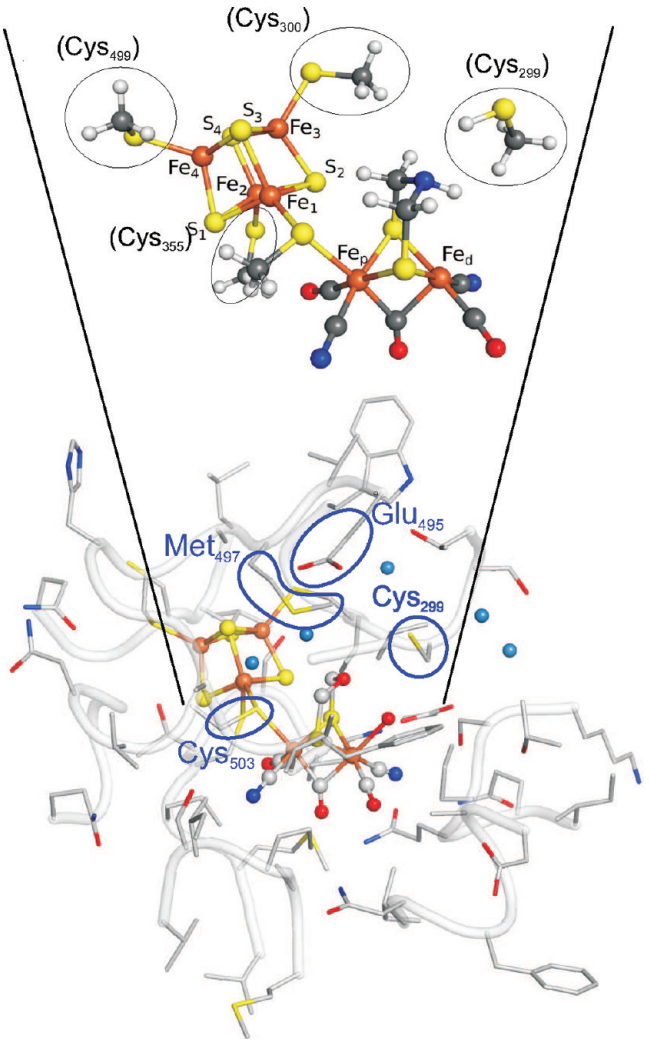

Figure 1. (top) Structure of the H cluster model studied in this work. Element color code: red, O; gray, C; blue, N; yellow, S; brown, Fe; white, H. The introduced numbering of the iron atoms is used consistently through the paper. (bottom) The H cluster in the crystal structure of [FeFe] hydrogenase from *C. pasteurianum* (PDB entry 3C8Y[33]). Water molecules from the crystal structure that connect the two subclusters are depicted as blue spheres.

described in ref 27: i.e., cysteine ligands have been replaced by thiomethanolate molecules where one C−H bond was spatially fixed according to the C_α−C_β bond as observed in the crystal structure of the [FeFe] hydrogenase of *Cl. pasteurianum*.[33] We focus on the active oxidized form H_{ox}^{cat} of the H cluster with a total electric charge set to 3− elementary charges. In nature, the high negative charge of the active site is compensated by the protein scaffold. In the case of our model, the continuum solvation model COSMO[34] was used to mimic electrostatic effects, which would otherwise be induced by the protein environment, and to minimize charge artifacts, which could arise when species with different charges are compared. EPR studies show that the H_{ox}^{cat} form of the enzyme should correspond to a doublet state.[3] In order to obtain more insight into the spin-dependent reactivity of the H cluster, we also compare with results obtained for the quartet state.

For our study of the reactivity of the isolated H cluster with oxygen species, we should, however, keep in mind which atoms

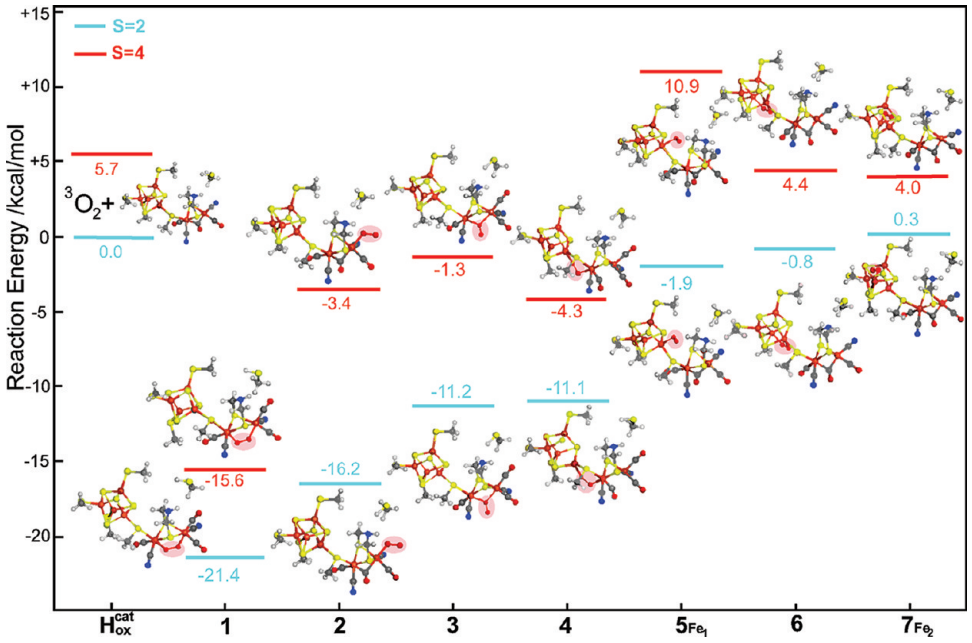

Figure 2. Comparison of different possible dioxygen adducts of the active *oxidized* H_{ox}^{cat} form of the H cluster (total charge is 3− elementary charges). The structures have been optimized with BP86/RI/TZVP/COSMO in order to account for the high negative charge. All clusters are described in doublet (blue) and quartet (red) spin states. The point of zero-energy reference has been chosen as the free $^3O_2$ and the isolated H_{ox}^{cat} form. Shaded ovals highlight the coordinated O_2 molecule. Element color code: red, O; gray, C; blue, N; yellow, S. brown, Fe; white, H.

of the H cluster are spatially accessible for the dioxygen species. For this purpose, we first assess the space available for oxygen moving along the H cluster *when embedded in the protein*. The published crystal structures of [FeFe] hydrogenase generally feature a high content of crystal water molecules, especially in the vicinity of the H cluster. Figure 1 shows a water-filled path present in the crystal structure of the [FeFe] hydrogenase from *C. pasteurianum* that connects the $2[Fe]_H$ subcluster and the associated cubane. This could facilitate the diffusion of reactive oxygen species, provided the dynamics of the protein allows for subtle rearrangements of side chains such as Cys_{299} and Met_{497} (Figure 1). Unfortunately, no crystal structure exists for the hydrogenase from *C. reinhardtii*, for which the oxidative damage of the cubane was proposed,[29] but the high degree of sequence similarity between the clostridial and the algal protein suggests the presence of a similar hydrophilic channel also for the enzyme from *C. reinhardtii*. This is also supported by the crystal structure of a $2[Fe]_H$ subcluster-free form of this hydrogenase.[35] Therefore, water-filled tracks around the H cluster where single water molecules can be displaced by reactive oxygen species (ROS) appear to be an effective means by which these compounds can reach the $[Fe_4S_4]$ moiety.

2.1. $^3O_2$ Binding Sites. If we now consider oxygen species moving along the H cluster, we must first study possible binding sites. Figure 2 compares the reaction energies for the formation of different O_2 adducts of the H cluster in the H_{ox}^{cat} form and confirms[23,32] that the $2[Fe]_H$ subsite is the primary site of O_2 attack also for thermodynamic reasons (apart from the kinetic reason that it is the first site reached from the gas diffusion channel). To compare all isomers, we choose the added energies of $^3O_2$ and the isolated H_{ox}^{cat} form as energy reference. In the BP86 calculations, the low-spin (doublet) state is always energetically favored over the quartet state (see Figure 2), irrespective of the O_2 adduct formed. However, care must be taken in all cases where the quartet state is close in energy, because pure density functionals such as BP86 favor low-spin states over high-spin states and the ordering might reverse when the energy gap for a given species is small.[36−38] However, this would then hardly change the overall energetic picture of the reactions considered. Consequently, it is well justified to assume a $2[Fe]_H$ subsite oxygen adduct as a starting structure and to investigate possible subsequent reaction events that lead to an irreversible destruction of the H cluster.

As it is a priori not certain that the initial attack of O_2 on the H cluster takes place when the enzyme is in its oxidized form, we also considered formation of different O_2 adducts of the H cluster in the reduced H_{red}^{cat} form (Figure 3). Again, the $2[Fe]_H$ subsite is the primary site of O_2 coordination. Interestingly, the dioxygen adduct to the distal iron atom Fe_d of the $2[Fe]_H$ subsite is energetically the most favored one for the reduced form of the enzyme. To compare all isomers, we choose as energy reference $^3O_2$ and the isolated H_{red}^{cat} form. Here, for the oxygen adduct **6** in the reduced state, the triplet configuration is more stable than the singlet one because of a ligand rearrangement that occurs during structure optimization. Hydrogen bonding from the NH group of the dithiomethylamine (dtma) bridge of the dinuclear subsite to the CN^- ligand of the iron atom Fe_d is responsible for stabilizing this adduct, although this is not likely to happen in the protein environment and is thus an artifact of our minimal model system.

2.2. Possibility for Catalytic Formation of Reactive Oxygen Species. In the previous work published by our group, we studied a series of protonation events and water abstraction that could possibly lead to a breakdown of the $2[Fe]_H$ subsite.[23] However, for the [FeFe] hydrogenase of *Cl. pasteurianum* the aforementioned experimental data of Armstrong, Happe, and co-workers[29] suggest decomposition of the $[Fe_4S_4]$ cubane following the conversion of the coordinating O_2 to a reactive oxygen species (ROS).

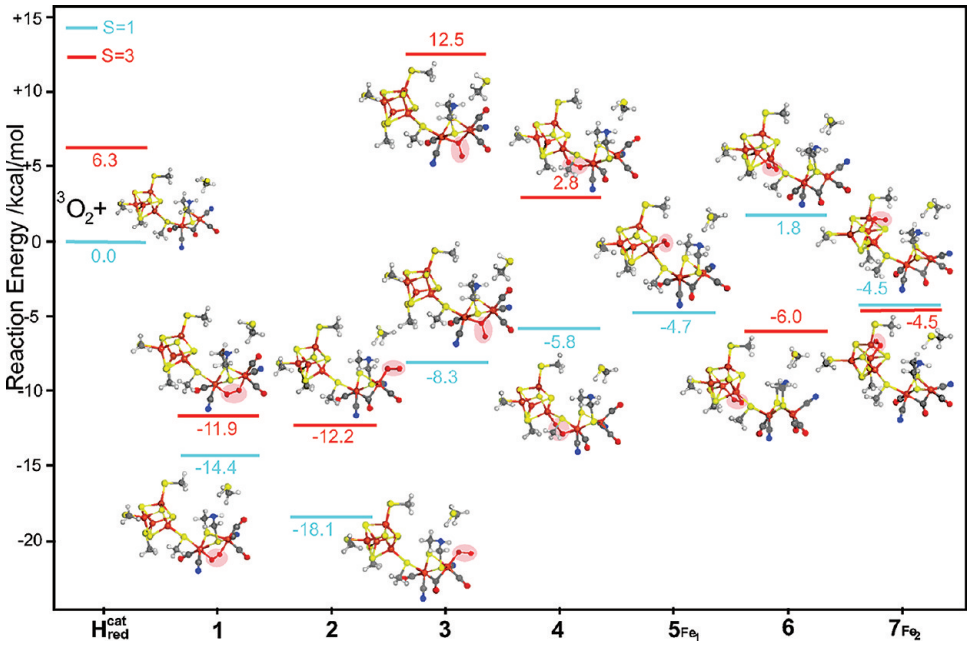

Figure 3. Comparison of different possible dioxygen adducts of the active *reduced* H_{red}^{cat} form of the H cluster (total charge is 4− elementary charges). The structures have been optimized with BP86/RI/TZVP/COSMO, and for the sake of simplicity, we use the same numbering of structures as in the case of the oxidized form in Figure 2. All clusters are described in singlet (blue) and triplet (red) spin states. The point of zero-energy reference has been chosen as the free $^3O_2$ and the isolated H_{red}^{cat} form. Shaded ovals highlight the coordinated O_2 molecule. Element color code: red, O; gray, C; blue, N; yellow, S; brown, Fe; white, H.

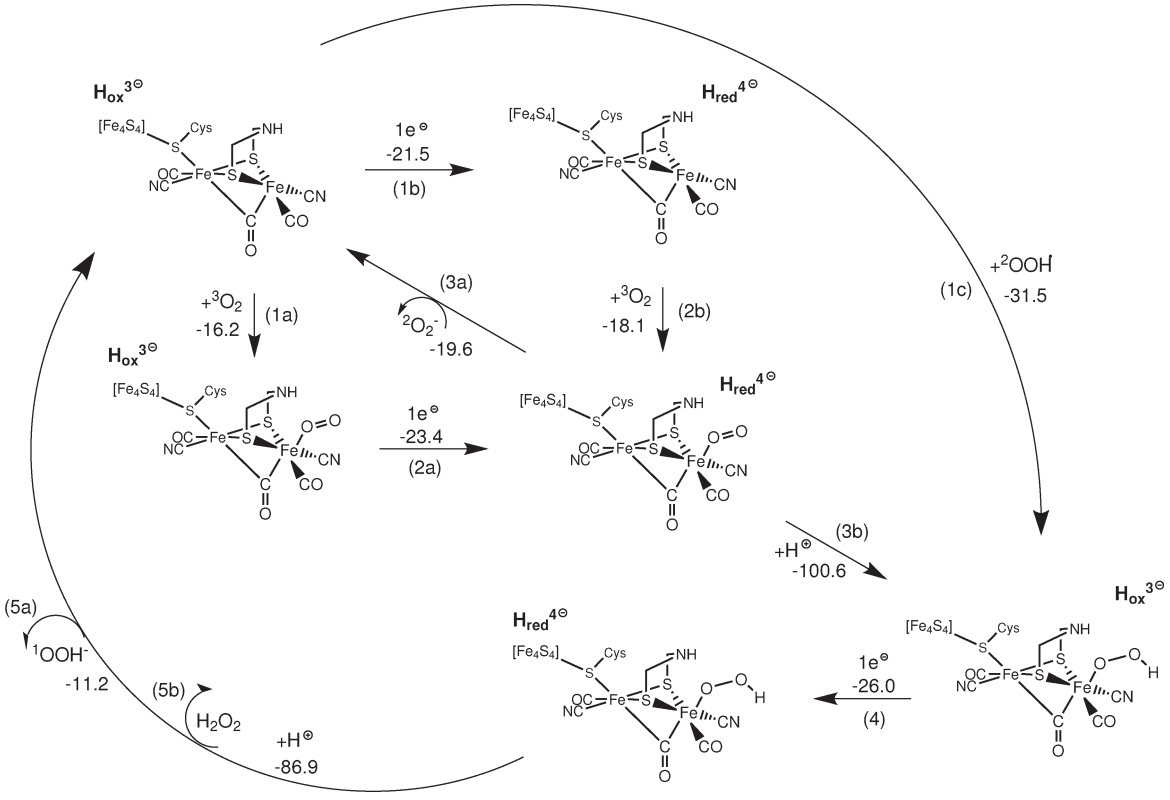

Figure 4. Possible catalytic reaction cycle for the formation of reactive oxygen species (ROS) at the H cluster. The given charges correspond to the active oxidized H_{ox}^{cat} and the active reduced H_{red}^{cat} forms of the H cluster. All clusters are considered to be in low spin state. Reaction energies in kcal/mol are calculated for fully optimized structures (BP86/RI/TZVP/COSMO) with respect to the isolated H_{ox}^{cat} form and $^3O_2$, $^2O_2^-$, ^{2}OOH•, ^{1}OOH$^-$, $^1H_2O_2$, respectively. For reaction energies obtained with the B3LYP functional, see Table 1. Protonation energies were calculated by assuming an energy of −262.4 kcal/mol for a solvated proton.[39,40]

dx.doi.org/10.1021/ja209165r |*J. Am. Chem. Soc.* 2011, 133, 20588–20603

Table 1. Reaction Energies for the Reactions Shown in Figure 4 with the Active Oxidized H_{ox}^{cat} and the Oxidized Inactive H_{ox}^{inact} Forms of the H Cluster as the Starting Points[a]

	H_{ox}^{cat}—H_{red}^{cat}		H_{ox}^{inact}—H_{ox}^{cat}	
reacn	BP86	B3LYP	BP86	B3LYP
1a	−16.2	−8.6	−13.6	−6.0
2a	−23.4	−23.5	−58.4	−81.4
1b	−21.5	−10.3	−55.8	−78.8
2b	−18.1	−21.9	−16.6	−8.6
3a	−19.6	−25.5	+12.9	+29.7
$3b^{ext}$	−100.6	−99.4	−66.6	−50.1
$3b^{int}$	−2.2	+16.8	+8.5	+19.8
1c	−31.5	−23.9	−30.0	−23.9
4	−26.0	−27.0	−57.4	−72.9
5a	−11.2	−16.4	+18.6	+35.4
$5b^{ext}$	−86.9	−89.3	−60.9	−60.5
$5b^{int}$	+6.9			

[a] B3LYP energies (kcal/mol) were obtained for single-point calculations with the COSMO solvation model (ε = 4) on BP86/RI/TZVP/COSMO optimized structures. Protonation energies marked with the superscript "ext" were calculated by assuming, for a solvated proton, an energy of −262.4 kcal/mol.[39,40] For comparison, the energies for internal protonation with proton transfer from Cys_{299} are marked with the superscript "int". In the case of $5b^{int}$ and H_{ox}^{inact}—H_{ox}^{cat} the proton moves back to the cysteine in our structure optimization with tight convergence thresholds.

As reported previously, $^3O_2$ addition to the distal Fe_d atom of the $2[Fe]_H$ subsite in the present model cluster is exothermic by −17.5 kcal/mol[27] (here, we find a slightly different value of −16.2 kcal/mol, as we have applied tighter convergence thresholds throughout; see Appendix). If the H_{ox}^{cat} form of the enzyme is considered (see Figure 2), the coordinated O_2 ligand in **2** features an O−O bond length of 1.31 Å, which points to the superoxide species O_2^- in support of the hypothesis by Armstrong, Happe, and co-workers.[29] Here, we find that dissociation of the bound superoxide from the Fe_d atom is endothermic by +12.7 kcal/mol and is therefore unlikely to occur.

This situation changes if a one-electron reduction of the cluster is considered which is energetically favored by −21.5 kcal/mol and leaves an overall charge of 4− elementary charges on the H cluster, corresponding to the H_{red}^{cat} form. Notably, the release of O_2^- in this redox state is exothermic by −19.6 kcal/mol. As an alternative to O_2^- release, a protonation of the terminal oxygen atom of the attached O_2 species could precede a dissociation of $OOH^•$. With Cys_{299} (nomenclature of the enzyme from *C. pasteurianum*) as proton donor, we obtain a slightly exothermic reaction energy of −2.2 kcal/mol. However, we find the dissociation of $OOH^•$ to be endothermic by +31.5 kcal/mol for the H_{ox}^{cat} form and by +36.0 kcal/mol for the H_{red}^{cat} form, respectively. Therefore, in terms of reaction energies reduction and superoxide release from the H cluster in H_{red}^{cat} form is the only feasible way to produce O_2^- at the catalytic center. Remarkably, these results suggest that a catalytic cycle for the formation of superoxide can be proposed, provided that rereduction of the H cluster can still be sustained by suitable electron donors (see Figure 4).

Interestingly, when one considers further protonation and reduction events, the formation of H_2O_2 and OOH^- also appears to be feasible at the $2[Fe]_H$ subsite, as the scheme shown in Figure 4 demonstrates. In this case protonation of the reduced adduct **2** (total charge is 4− elementary charges) can take place as a competing pathway to O_2^- release. This induces reduction of the superoxide ligand to a peroxide-like species, as can be deduced from the increased oxygen−oxygen bond length of 1.47 Å. We study the protonation reaction both by considering the transfer of an external solvated proton and by choosing Cys_{299} as the proton donor (see Table 1). Protonation is exothermic by −100.6 kcal/mol if a solvated proton is considered and by −2.2 kcal/mol for the internal proton transfer from Cys_{299}. Subsequent reprotonation of Cys_{299} is energetically favored by −98.4 kcal/mol (external protonation by a solvated proton).

A subsequent reduction of the active site by one electron is then exothermic by −26.0 kcal/mol and can be followed by one of two reaction events that close the catalytic cycle for peroxide formation. The first possibility is release of a OOH^- ion (−11.2 kcal/mol), which can be later protonated to finally form H_2O_2. The second option is protonation of the OOH adduct to form H_2O_2, which is found to spontaneously dissociate from the active site. The reaction energy for this step is −86.9 kcal/mol for the addition of H^+ from solution and +6.9 kcal/mol if Cys_{299} is considered as a proton donor. Hence, the former possibility appears to be more likely.

A final reprotonation of the cysteine residue 299 is again exothermic by −93.7 kcal/mol. Both reaction paths close the catalytic cycle, leaving the active site in its oxidized, catalytically active form H_{ox}^{cat}. Interestingly, H^+ transfer from Cys_{299} to the OOH adduct cannot take place before the system is reduced by one electron, because otherwise the proton returns back to the sulfur atom of the cysteine residue in the course of structure optimization. Hydrogen peroxide can also be formed by rebinding of protonated O_2^- to the distal iron atom (H_{ox}^{cat} redox state of the cluster), which is exothermic by −31.5 kcal/mol, and can be followed by the same reaction events as described previously starting with the one-electron reduction of the system. On the basis of the reaction scheme proposed in Figure 4, production of O_2^- and OOH^- appears to be a feasible toxic pathway catalyzed by the H cluster.

The surprising observation[2] of O_2 tolerance of the otherwise extremely oxygen sensitive [FeFe] hydrogenase in its anaerobically generated inactive form H_{ox}^{inact} can now be explained. Let us consider Figure 4 (for reaction energies see Table 1) with a starting charge state of the H cluster of 2− instead of 3− elementary charge. The first step—coordination of an oxygen molecule to the Fe_d atom—is less exothermic than for the H_{ox}^{cat} form (−13.6 kcal/mol) but still feasible. However, all subsequent steps involving proton transfer from Cys_{299} are not likely to occur. The proton returns to Cys_{299} when internal protonation is considered or, when considering a solvated proton (see reactions 3b and 5b in Table 1), the protonation is almost 30 kcal/mol less exothermic than for the H_{ox}^{cat} form of the enzyme. The alternative pathway with O_2^- release (reaction 3a) is endothermic by +12.9 kcal/mol. Finally, the dissociation of OOH^- (reaction 5a) is endothermic by +18.6 kcal/mol. Therefore, for the anaerobically prepared H_{ox}^{inact} state, the formation of ROS at the $2[Fe]_H$ subsite is not likely and cannot lead to irreversible cluster destruction.

Finally, we should note that the reaction energies obtained with the B3LYP functional (given in Table 1) are in line with the BP86 data discussed.

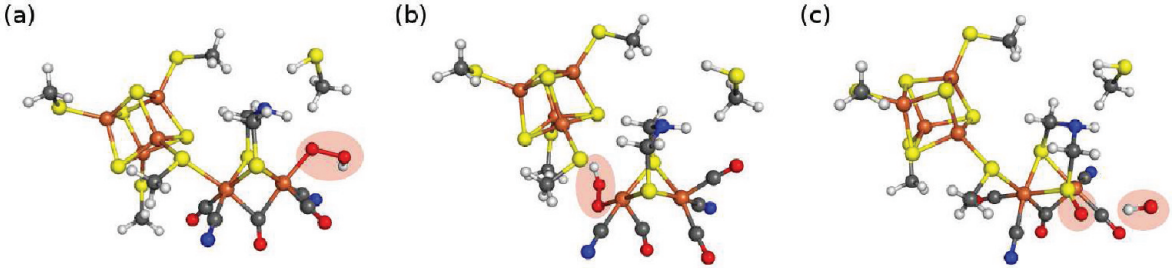

Figure 5. Structures of OOH adducts of the $2[Fe]_H$ subsite optimized with BP86/RI/TZVP/COSMO for a total charge of 3− elementary charges in all cases: (a) distal adduct; (b) proximal adduct; (c) oxidized dtma ligand. The clusters are considered in their low spin states (singlet). Shaded ovals highlight coordinated $OOH^•$ or reaction products thereof.

2.3. Possible Oxidants. Summarizing what we have found so far, triplet O_2 binds to the distal iron atom of the H cluster and can exothermically be transformed into superoxide or hydroperoxide anion. Thereafter, O_2^- and OOH^- can be protonated to become an $OOH^•$ radical and H_2O_2, respectively. Such protonation events can be facilitated in principle by protic residues such as cysteine, tyrosine, histidine, and glutamic acid. For these amino acids we calculate +8.5, +6.6, −40.4, and −4.4 kcal/mol, respectively, for proton transfer from an isolated amino acid to O_2^- to form $OOH^•$. Analogously, for proton transfer from cysteine, tyrosine, histidine, and glutamic acid to OOH^- to form H_2O_2, we obtained −14.7, −16.5, −63.5, and −27.6 kcal/mol, respectively. Hence, protonation of O_2^- from a cysteine is unlikely to occur, while a protonated histidine or glutamic acid in the vicinity of the H cluster could accomplish this. However, there is no histidine residue in the cluster environment but glutamic acid (Glu_{495}) is located in close proximity to the active site and could in principle act as a proton donor. In contrast, protonation of OOH^- from any of the residues considered (leaving an anionic residue behind) is very exothermic and thus likely to take place. The cysteine residue Cys_{299} is located just above the postulated site of OOH^- dissociation and could therefore easily act as a proton donor for the formation of H_2O_2. To determine which ROS species are most likely to attack the active site, it is important to note that O_2^- can undergo spontaneous disproportionation:[41]

$$2O_2^- + 2H_2O \rightarrow H_2O_2 + O_2 + 2OH^-$$

This is the fourth possible way to produce H_2O_2 around the cluster. Therefore, hydrogen peroxide appears to be the most convincing reactant that could be responsible for the irreversible inhibition of the H cluster. Nevertheless, we continue to investigate the action of all four reactive oxygen species which can be catalytically produced at the active site: O_2^-, $OOH^•$, OOH^-, and H_2O_2.

At first, we study the coordination of the negatively charged species O_2^- and OOH^-. Superoxide adducts to the H cluster are presented in Figure 3 for O_2 addition, but the formation is always impeded by endothermic reaction energies (not shown). For instance, the energetics of O_2^- coordination to the Fe_1 and Fe_2 atoms of the cubane in the H_{ox}^{cat} state of the cluster (see adducts $\mathbf{5}_{Fe_1}$ and $\mathbf{7}_{Fe_2}$ in Figure 3) are +33.0 and +33.2 kcal/mol. All attempts to coordinate O_2^- to a sulfur atom of the cubane resulted in dissociation of the superoxide, leaving the cluster intact. In general, formation of OOH^- adducts at iron or sulfur atoms of the cubane is endothermic by more than +20 kcal/mol.

As a consequence, we consider O_2^- and OOH^- to be important in the migration step from the distal iron atom toward the cubane cluster, as these species can dissociate from the distal iron atom. Thus, reaction at the cubane most likely occurs only when superoxide is protonated to yield $OOH^•$ or again reduced to form H_2O_2. Therefore, we now exclude O_2^- and OOH^- for the subsequent mechanism of H cluster inhibition.

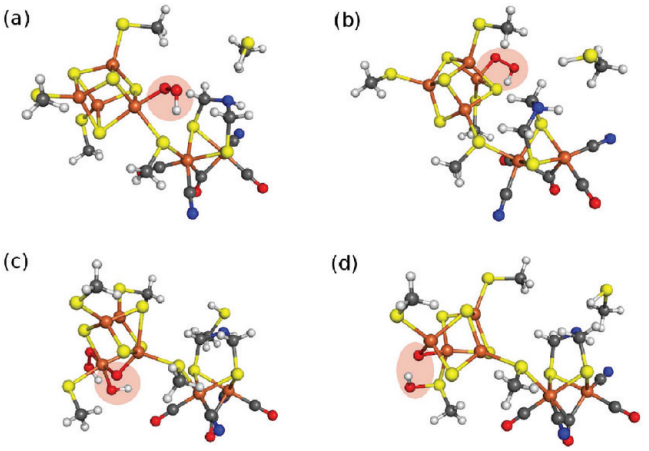

Figure 6. Structures of $OOH^•$ coordination to the Fe_1 (a) and Fe_2 (b) iron atoms of the $[Fe_4S_4]$ cubane, $\mathbf{Fe_1}$**-OOH** and $\mathbf{Fe_2}$**-OOH**, respectively, optimized with BP86/RI/TZVP/COSMO (see Figure 1 for the labeling of atoms). Structure $\mathbf{Fe_2}$**-OOH(OH)(**μ**-O)** depicted in (c) was obtained after coordination of a second $OOH^•$. Structure $\mathbf{Fe_2}$**-(**μ**-O)[(S)OH]** in (d) emerges after activation of the $OOH^•$ bound in $\mathbf{Fe_2}$**-OOH** by bending the FeOO angle. The charge is 3− elementary charges in all cases. The clusters are described in the low-spin states. Shaded ovals highlight the coordinated $OOH^•$ molecule.

3. THE $OOH^•$ RADICAL AS DAMAGING AGENT

As already outlined above, the direct attack of O_2 or O_2^- at the $[Fe_4S_4]$ cubane is almost thermoneutral and therefore cannot explain the decomposition of the H cluster. This situation changes dramatically when we consider the protonated superoxide ion that yields the radical $OOH^•$.

While we are primarily interested in reactions that take place at the cubane subcluster, we should briefly discuss what $OOH^•$ can induce at the dinuclear iron subsite. Simple rebinding of superoxide in the protonated $OOH^•$ form to the distal iron atom Fe_d of the $2[Fe]_H$ subsite (Figure 5a) is energetically favored by −31.5 kcal/mol and can be—next to the $OOH^•$ binding to the proximal iron atom Fe_p (Figure 5b) with a reaction energy of −26.7 kcal/mol—the preferred site of $OOH^•$ coordination to the active site. The OOH ligand can then be further reduced and may dissociate as hydrogen

dx.doi.org/10.1021/ja209165r |J. Am. Chem. Soc. 2011, 133, 20588–20603

peroxide, as shown in the scheme of Figure 4. It is also possible that $OOH^{\bullet}$ oxidizes sulfur atoms from the dtma ligand linking the two irons of the $2[Fe]_H$ subsite. This reaction is exothermic by −20.4 kcal/mol; the product is depicted in Figure 5. Nevertheless, $OOH^{\bullet}$ reactions with the cubane will be of importance when the protonation of superoxide is facilitated in close proximity to the cubane rather than to the $2[Fe]_H$ subsite, which is the case when Glu_{495} is considered as the proton donor. Note that Figure 5b shows a structure where the $S-Fe_p$ bond, which links the subsite to the cubane through Cys_{503}, is cleaved. A similar process has been found in the context of the inhibitor CO reacting with the H cluster.[42]

Note that the variety of additions and reaction events which can follow the initial $OOH^{\bullet}$ coordination to the cubane is too large to be investigated systematically. For example, three options exist to approach a single iron center by the $OOH^{\bullet}$ species. Some adducts feature intact cubane clusters, while in others the cubane is opened. These structures are very similar in energy (within a range of up to 3 kcal/mol). Here, we report an intact cubane structure for **Fe_1-OOH** and an open one for **Fe_2-OOH** (see Figure 6). All other structures obtained are presented and discussed in detail in the Supporting Information.

Coordination of $OOH^{\bullet}$ to iron atom Fe_1 of the cubane, for instance, is exothermic by −18.6 kcal/mol, with similar energies to be found for the addition to the remaining three Fe atoms.

We now proceed to investigate possible pathways for irreversible cubane disintegration following $OOH^{\bullet}$ attack. First, we study the addition of a second $OOH^{\bullet}$ species to the newly formed free coordination site at iron atom Fe_2 in **Fe_2-OOH**, which resulted after cleavage of an iron−sulfur bond upon attack of the first $OOH^{\bullet}$ radical. Structure optimization of this species yields **Fe_2-OOH(OH)(μ-O)** (Figure 6c) featuring a broken O−OH bond with an energy of −51.5 kcal/mol for

$$OOH^{\bullet} + \mathbf{Fe_2-OOH} \rightarrow \mathbf{Fe_2-OOH(OH)(\mu-O)}$$

In **Fe_2-OOH(OH)(μ-O)**, the oxo bridge is formed between Fe_2 and Fe_4 (see Figure 1 for the labeling of atoms).

Another possible decomposition pathway of the $[Fe_4S_4]$ cubane may open up in an intramolecular reaction, when we distort (activate) the optimized structure of the OOH adduct **Fe_2-OOH** by decreasing the O···S distance with respect to the coordinating cysteine. If it is considered as an elementary reaction, this distortion may require an activation energy that is too high to be thermally activated. However, structure optimization of a distorted species with an O−S distance of 1.6 Å results in splitting of the O−OH bond and significant distortion of the cubane in the structure **Fe_2-(μ-O)[(S)OH]**, in which the OH fragment binds to a sulfur atom (see Figure 6d). These structural changes are accompanied by an overall exothermic reaction of −38.0 kcal/mol. Attempts to locate transition states for such a reaction turned out to be very difficult. Nevertheless, these attempts have led us to the conclusion that a direct intramolecular attack in an elementary (one-step) reaction requires an energy that is too high to be important for cluster decomposition reactions. However, such an intramolecular decomposition reaction does not need to be considered as an *elementary* reaction step. Instead, it may be feasible if it proceeds stepwise.

In order to explore this latter option, we calculated the intrinsic bond energies of O−O and Fe−S in **Fe_2-OOH**: i.e., the electronic energy differences for bond breaking if the products are taken in the structure they adopt in **Fe_2-OOH**. These (intrinsic) reaction energies for structurally frozen fragments are a good estimate for an activation barrier of such a bond-breaking reaction which produces two independent molecular fragments. We obtained an intrinsic bond energy of 37.5 kcal/mol for the O−O bond and of 26.9 kcal/mol for the Fe−S bond (remember that we break the Fe−S bond to the Fe atom which already coordinates the OOH species). Hence, to first activate the Fe−S bond appears to be feasible and a subsequent structure optimization shows that the actual dissociation energy is only +0.8 kcal/mol for breaking the Fe−S bond with subsequent structural relaxation to yield the intermediate **Fe_2-OOH···[S]** (for the sake of comparison, taking structural relaxation in the O−O bond breaking of **Fe_2-OOH** into account reduces the endothermicity of this process only to +26.7 kcal/mol). The Fe−S bond-breaking step is thus basically thermoneutral and can be considered a first step toward the production of **Fe_2-(μ-O)[(S)OH]**. In order to understand whether subsequent steps are also feasible, we calculated the dissociation of OH from the intermediate **Fe_2-OOH···[S]** to form the second intermediate **Fe_2-O···[S]**, which requires an energy of only +24.0 kcal/mol. The reaction of this dissociated OH radical with the noncoordinating sulfur atom of the second intermediate **Fe_2-O···[S]** to yield the final product **Fe_2-(μ-O)[(S)OH]** is exothermic by −31.8 kcal/mol.

As a final remark, we note that the energy for coordination of a second $OOH^{\bullet}$ to Fe_3 in the distorted cubane **Fe_2-(μ-O)-[(S)OH]** is −17.7 kcal/mol. Note that the reaction energy for an addition of a second $OOH^{\bullet}$ to Fe_1 in the intact cubane of **Fe_1-OOH** is exothermic by −21.7 kcal/mol, while the coordination of a second $OOH^{\bullet}$ to Fe_4 of **Fe_1-OOH** yields −25.5 kcal/mol.

Addition of further $OOH^{\bullet}$ radicals are exothermic and lead to even more pronounced structural changes of the iron−sulfur cluster. It is clearly visible that already the $[Fe_4S_4]$ unit of the structure depicted in Figure 6d is no longer of cuboidal shape. This structural deformation is in line with the fact of changed iron−sulfur distances observed in the X-ray absorption spectroscopy (XAS) spectra of [FeFe] hydrogenase after oxygen exposure[29] with a still intact $2[Fe]_H$ subsite.

Release of an iron atom from an oxidized $[Fe_4S_4]$ cubane was proposed as a possible decomposition pathway for the iron−sulfur cluster of the enzyme aconitase.[30] At this stage, it is not possible to decide whether the iron atom Fe_2 can be dissolved, but we may refer to the analogous case in the next section on sulfoxygenation. It is, however, reasonable that the final structure, which is a result of a highly exothermic reaction, may release a solvated iron ion.

Clearly, the uncharged $OOH^{\bullet}$ is much more reactive than superoxide and $OOH^{\bullet}$ binding could account for the irreversible destruction of the cubane. The $OOH^{\bullet}$ radical is known to be very reactive and usually is created shortly before the actual reaction takes place. The presented results confirm that $OOH^{\bullet}$ is capable of $[Fe_4S_4]$ cubane decomposition, provided that protonation of superoxide to produce this highly reactive species can be accomplished near the cubane.

4. SULFOXYGENATION

The catalytic formation of hydrogen peroxide at the distal iron atom opens the possibility for several competing decomposition reactions at the active center. It is well-known that H_2O_2 can oxidize thiolate and thioether sulfur atoms. Hence, it is no surprise that the formation of oxidized cysteines, i.e., of CysSO groups, was also suggested for the oxidized form of [NiFe]

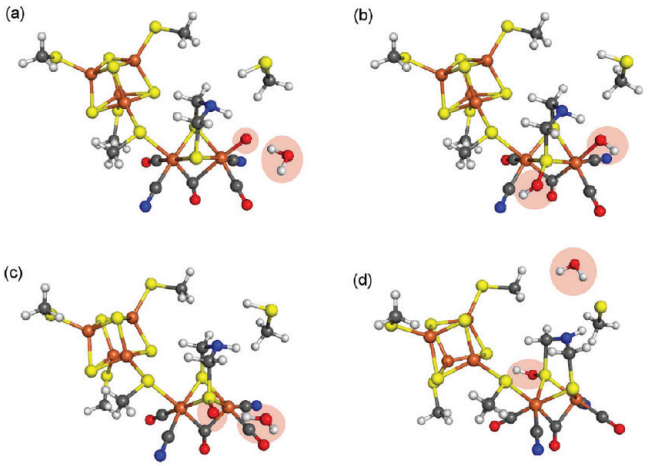

Figure 7. Reaction products of hydrogen peroxide addition to the $2[Fe]_H$ subcluster. Structures were optimized with BP86/RI/TZVP/COSMO considering a total charge of 3− elementary charges in all cases. The clusters are described in their low-spin states (doublet). Shaded ovals highlight the oxygen-based reaction products.

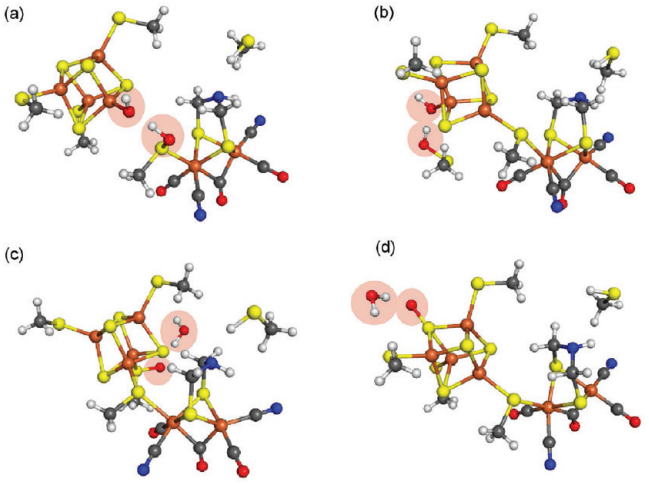

Figure 8. Reaction products for the addition of hydrogen peroxide to cysteines coordinating the $[Fe_4S_4]$ cubane: (a) product $\mathbf{I}_{Fe1}$ of H_2O_2 addition to Cys_{503}; (b) $\mathbf{I}_{Fe2}$ for H_2O_2 addition to Cys_{355}; (c) $\mathbf{II}_{Fe2}$ to Cys_{355}; (d) product $\mathbf{I}_{Fe3}$ of H_2O_2 addition to Cys_{300}. Structures were optimized with BP86/RI/TZVP/COSMO for a total charge of 3− elementary charges in all cases. The clusters are considered to be in their low-spin states (doublet). Shaded ovals highlight the oxygen-based reaction products.

hydrogenase on the basis of a combined XAS, EPR, Fourier transform infrared (FTIR) spectroscopy, and broken-symmetry (BS) DFT study.[17] Such reactions can also take place in the vicinity of the H cluster. For this section we optimized possible reaction products of H_2O_2 attack by placing this molecule in the close vicinity of various atoms of the H cluster. Of course, this may create high-energy structures that can then relax by O−O bond cleavage.

We should stress that H_2O_2 does not bind to the distal Fe_d iron atom of the $2[Fe]_H$ subsite in the H_{ox}^{cat} state. If we place H_2O_2 in close vicinity of Fe_d, the proton moves from the oxygen atom proximal to Fe_d to the second O atom such that water is formed with a reaction energy of −35.6 kcal/mol. The remaining

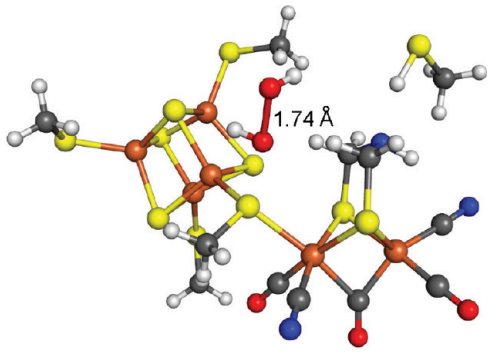

Figure 9. Transition state for the reaction of H_2O_2 with the subcluster-bridging S atom of Cys 503 (*C. pasteurianum*).

oxygen atom is then a ligand to Fe_d (see top left structure in Figure 7 and compare also ref 23). The water formation reaction, however, is 8 kcal/mol less exothermic than the competing oxidation of the thiolate sulfur atoms, which can take place either at the dtma bridge directly connected to the distal iron atom Fe_d or at the closest cysteine residue Cys_{503}. Since both the distal iron atom and the sulfur atoms are easily accessible for H_2O_2, the more exothermic reactions with thiolates are more likely to take place than the oxidation of the iron atom Fe_d. The latter reaction would lead to the competing degradation pathway discussed in the previous study reported by our group.[23]

Generally, we observe that H_2O_2 preferentially binds and reacts with thiolate groups, while we were not able to converge adducts of H_2O_2 with Fe atoms of the cubane. Sulfur atoms of the $[Fe_4S_4]$ subsite are also not likely to be the primary site of H_2O_2 attack, because in all calculations performed H_2O_2 dissociates from the cluster during structure optimization, indicating that the cluster would at least require activation, if feasible at all. This result is in line with the observation of the sensitivity of charged Cys residues against H_2O_2. However, a sulfur atom at the cubane might be oxidized to form a sulfoxide compound after H_2O_2 is first placed close to a thiolate group of a coordinating cysteine ligand (see Figure 8d).

From the proposed site of H_2O_2 formation at the distal Fe_d iron atom, the thiolate groups that are most easily accessible belong to the bidentate dtma ligand. Here, H_2O_2 brought in close proximity to the dtma bridge leads to three different products, depending on the initial possible structure from which a calculation was started. The parameter that can be chosen completely freely upon attack of H_2O_2 to the dtma bridge is the dihedral angle among the oxygen atoms of hydrogen peroxide, the sulfur atom of the dtma bridge, and the distal iron atom Fe_d. The most exothermic among the products obtained (−43.2 kcal/mol) converges by cleavage of the O−O bond and water formation, while the sulfur atom is oxidized to a sulfoxide group (see Figure 7). Importantly, these results are obtained upon structure optimization without any activation of the H cluster.

For a complete picture of the attack of bridging sulfur atoms by H_2O_2, we need to investigate transition-state barriers. Figure 9 shows a transition state for the reaction of H_2O_2 with the subcluster-bridging sulfur atom of cysteine 503. The transition state was obtained by starting from an optimized structure of the free H cluster with overall charge of 3− elementary charges and varying the distance between one H_2O_2 O atom and the bridging sulfur atom between 1.67 and 2.57 Å. For each case a full structural optimization was carried out while the Cartesian

dx.doi.org/10.1021/ja209165r |*J. Am. Chem. Soc.* 2011, 133, 20588–20603

coordinates of the oxygen and the sulfur atom were kept fixed. For the maximum energy structure a more refined search was carried out by varying the O−S distance between 2.25 and 2.45 Å. The structure that featured the highest energy was obtained for a O−S distance of 2.35 Å. A vibrational analysis of this structure revealed six imaginary frequencies (i179.44, i121.52, i119.62, i104.78, i68.04, and i46.71 cm^{-1}) with the second frequency corresponding to the O−O stretch vibration. The second normal mode was then considered in an eigenvector-following approach as implemented in the Turbomole package to search for the transition state (see Appendix). Here, convergence could only be achieved by fixing the O−S distance to 2.35 Å during the search. Care was taken to converge a broken-symmetry solution that corresponds to the experimentally observed spin coupling of the oxidized H cluster. Subsequent frequency analysis revealed two imaginary frequencies (i80.66 and i4.90 cm^{-1}), with the first one corresponding to the O−O stretching vibration and the second one being an artifact of the seminumerical analysis. For determination of the activation barrier using this approximate transition state the electronic energy was re-evaluated by employing the COSMO solvent screening model and assuming a dielectric constant of 4.0. The activation barrier is only 7.6 kcal/mol and provides a reasonable upper bound for the activation energy of H_2O_2-induced oxidation of the subcluster-bridging sulfur atom of cysteine residue 503 (according to the *C. pasteurianum* sequence). Hence, the reaction of H_2O_2 with bridging sulfur atoms is clearly kinetically feasible.

Oxidation of sulfur atoms from bridging thiolates in compounds biomimetic to the active site of [FeFe] hydrogenase was discussed in a recent review by Darensbourg and Weigand.[31] The molecular structures with oxidized sulfur atoms presented in their review are comparable to the structures predicted by our DFT calculations (Figure 7). However, our study shows that an alternative product can be formed that features a S−OH moiety at the dtma ligand. The second OH group of the attacking H_2O_2 forms a water molecule after protonation by Cys_{299} (see Figure 7d). The energy for this reaction is −36.5 kcal/mol. The least exothermic (−29.0 kcal/mol) reaction product that could be formed by the reaction of H_2O_2 with the dtma bridge consists of a S−OH moiety and an OH ligand at the distal Fe_d atom (Figure 7b).

After the dtma ligand, the next accessible thiolate group is at the cysteine residue that connects the $2[Fe]_H$ subsite with the cubane (Cys_{503}). In this case, the most exothermic product (−40.8 kcal/mol) features a split O−O bond of H_2O_2 which is accompanied by breaking of the bond between the cysteine S atom and the Fe_1 atom of the cubane, thereby leaving oxidized S and Fe_1 atoms both carrying an OH group (mode $\mathbf{I}_{Fe1}$; see Figure 8a). Notably, for $[Fe_4S_4]$-carrying proteins as aconitase or HiPIPs (high potential iron−sulfur proteins) the formation of Fe−OH species is considered to be the initial step in $[Fe_4S_4]$ degradation, with the possibility that the oxidized iron atom can be dissolved by water, leading to the formation of a $[Fe_3S_4]$ cluster.[30] Interestingly, the type of reaction product obtained for the remaining three cysteines anchoring the $[Fe_4S_4]$ cluster depends on the corner of the cubane considered. At the site of the Fe_2 atom (compare Figure 1), which is coupled ferromagnetically to the Fe_1 atom in the H_{ox}^{cat} state of the active site, H_2O_2 can coordinate in mode $\mathbf{I}_{Fe2}$, similar to that described for the Fe_1 atom (see Figure 8), with a reaction energy of −42.4 kcal/mol. This type of product was not observed for cysteines connected to iron atoms Fe_3 and Fe_4. In contrast, when H_2O_2 attacks the sulfur atoms of cysteines coordinating iron atoms Fe_3 and Fe_4, it breaks into OH moieties and reattaches to the sulfur atoms from the cubane, oxidizing them as shown in Figure 8d. The byproduct of this reaction is water.

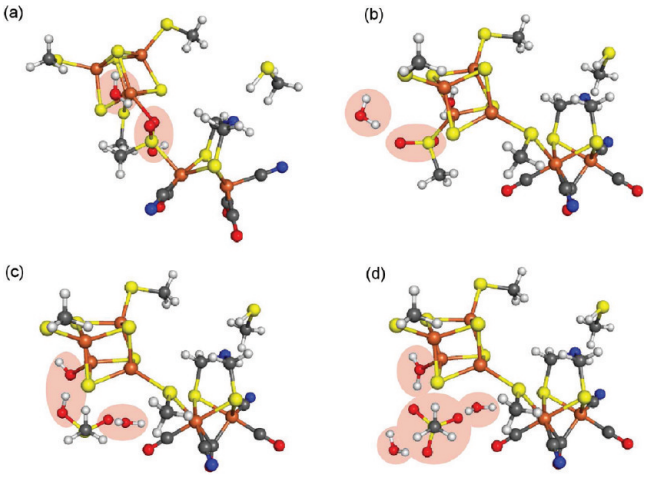

Figure 10. Reaction products for the addition of a second and a third H_2O_2 molecule to the H cluster: (a) addition of a second hydrogen peroxide to the oxidized sulfur atom of the structure $\mathbf{I}_{Fe1}$; (b, c) H_2O_2 addition to the sulfoxide of the structures $\mathbf{II}_{Fe2}$ (b) and $\mathbf{I}_{Fe2}$ (c); (d) final product of sulfoxygenation of the S atom. The total charge of the clusters is 3− elementary charges in all cases. The clusters are considered to be in their low-spin states (doublet). Shaded ovals highlight the oxygen-based reaction products. Note that the structure shown in (a) would differ substantially if the optimization was performed without the COSMO solvation model.

There is a possibility for an alternative adduct formation, common to all the cysteines coordinating the $[Fe_4S_4]$ cluster. As depicted in Figure 8c for Cys_{355}, H_2O_2 oxidizes the sulfur atoms to sulfoxide groups while the second oxygen atom is released as water. This type of reaction resembles the oxidation of the dtma ligand and delivers a similar overall reaction energy of −41.4 kcal/mol for the oxidation of Cys_{355}, with similar energies for the oxidation of the remaining cysteines. For the iron atom Fe_2 of the cubane, both binding modes $\mathbf{I}_{Fe2}$ and $\mathbf{II}_{Fe2}$ are energetically nearly degenerate, while for Fe_1 the preferred product is $\mathbf{I}_{Fe1}$. For Fe_4, oxidation of the sulfur atom of the coordinating cysteine residue is energetically preferable over oxidation of a sulfur atom of the cubane by almost 10 kcal/mol.

In contrast to the oxidized dtma ligand or sulfoxides formed at the cubane, the oxidized cysteine residues can be further oxidized by bringing a second H_2O_2 molecule into close proximity. This second reaction step results in formation of a sulfone and water and is somewhat more exothermic than the first step, with −59.8 kcal/mol for product $\mathbf{I}_{Fe2}$, −63.7 kcal/mol for $\mathbf{II}_{Fe2}$, and −61.7 kcal/mol for $\mathbf{I}_{Fe1}$ (see Figure 10). Of course, while doubly oxidized sulfur atoms, i.e., sulfones, are well-known oxidation products of thioethers, optimization of a transition-state structure would be needed to confirm that sulfone formation is possible under oxygen inhibition conditions.

If it would be kinetically possible to oxidize the sulfone for a third time, an $R-SO_3$ group bound to the protein would be produced which no longer can coordinate a metal atom of the H cluster. Then, another water molecule is coordinated to the iron atom Fe_2 of the cubane (see Figure 10d, where the $R-SO_3$ group

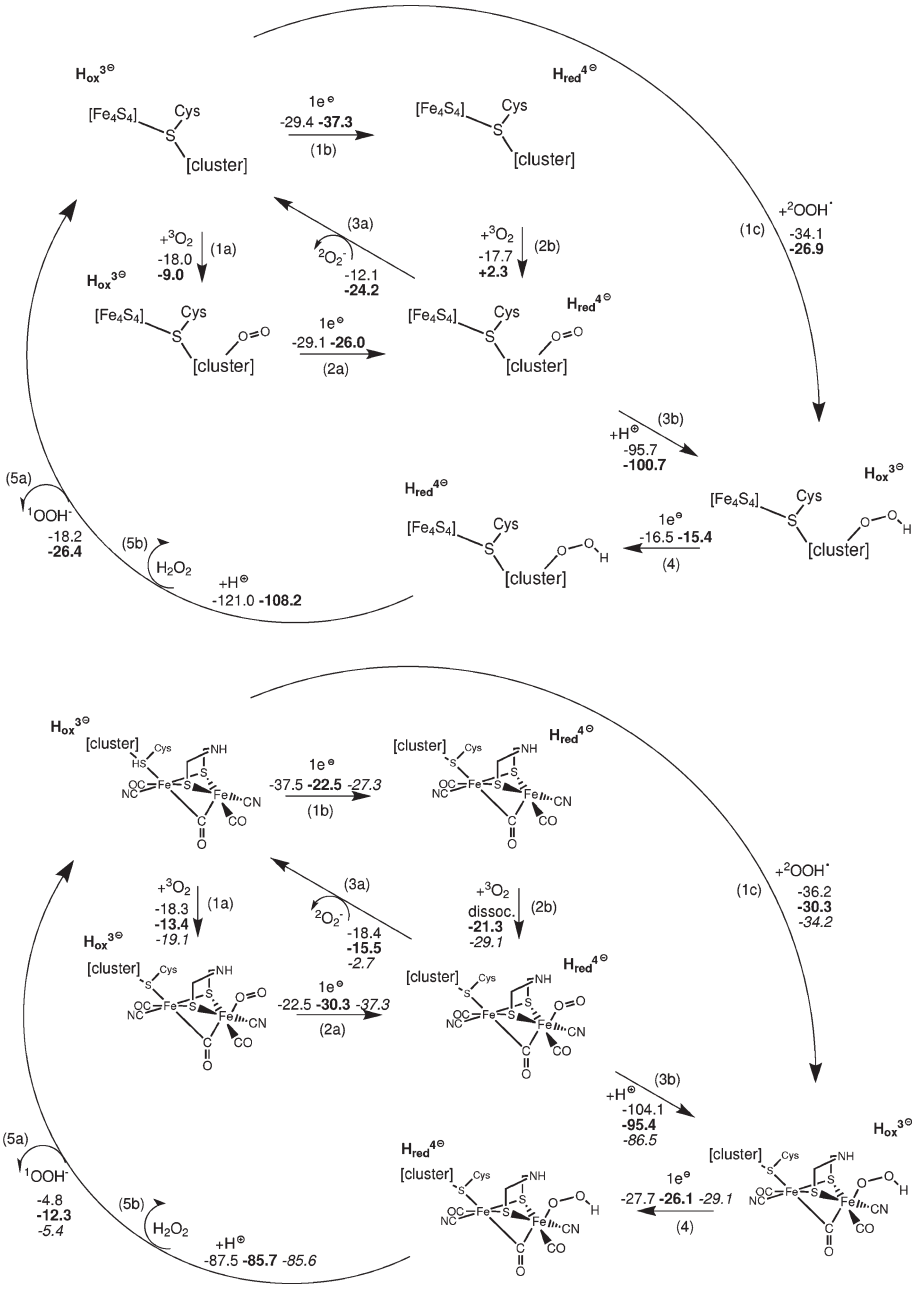

Figure 11. Reactions for the formation of ROS at the partially destroyed H cluster, where "[cluster]" represents either the structural unit of the reaction products **dtmaSO** and **dtmaSOH** presented in Figure 7c,d (top) or the structural unit of reaction products $\mathbf{I}_{Fe1}$, $\mathbf{Fe_2}$**-OOH**, and $\mathbf{Fe_2}$**-OOH(OH)**(μ**-O**) of Figure 8a and Figure 6b,c (bottom): Reaction energies (kcal/mol) for the top part corresponding to the starting structure **dtmaSO** are given in Roman type, while for the reaction cycle starting from the **dtmaSOH** structure, the reaction energies are given in boldface type. Reaction energies (kcal/mol) for the bottom part corresponding to the starting structure $\mathbf{I}_{Fe1}$ are given in Roman type, while for the reaction cycle starting from the $\mathbf{Fe_2}$**-OOH** structure, the reaction energies are given in boldface type. Reaction energies of $\mathbf{Fe_2}$**-OOH(OH)**(μ**-O**)-based clusters are given in italics. Protonation energies were calculated by assuming, for a solvated proton, an energy of −262.4 kcal/mol.[39,40] Given charges correspond to the active oxidized H_{ox}^{cat} and the active reduced H_{red}^{cat} forms of the modified H cluster. All clusters are considered in their low-spin state. Reaction energies are calculated for fully optimized structures (BP86/RI/TZVP/COSMO) with respect to $^3O_2$, $^2O_2^-$, ^{2}OOH•, ^{1}OOH$^-$, or $^1H_2O_2$ and **dtmaSO** and **dtmaSOH**, respectively (top), and with respect to $^3O_2$, $^2O_2^-$, ^{2}OOH•, ^{1}OOH$^-$, or $^1H_2O_2$ and $\mathbf{I}_{Fe1}$, $\mathbf{Fe_2}$**-OOH**, and $\mathbf{Fe_2}$**-OOH(OH)**(μ**-O**), respectively (bottom).

appears as Me−SO_3 in our structural model), which might subsequently be dissolved as mentioned before in the previous section on distingration induced by OOH•.

When we compare products of H_2O_2 addition to the H cluster with oxidation products that result from the attack of other ROS, we notice that the primary coordination preference that precedes subsequent reaction events is shifted from Fe to S atoms with increasing exothermicity in the series O_2, OOH•, H_2O_2. The oxidation energies for all reactions of hydrogen peroxide with thiolate groups are considerably more exothermic than for other reactive oxygen species and are close to −40 kcal/mol (for the first H_2O_2 addition). These results are in line with the work of Roth and Jordanov,[43] who showed that H_2O_2 readily decomposes model compounds of iron−sulfur cubanes in a much more

dx.doi.org/10.1021/ja209165r |J. Am. Chem. Soc. 2011, 133, 20588–20603

Table 2. Reaction Energies for the Reactions of Inhibited Forms of the H Cluster Shown in Figure *11*: i.e., dtmaSO, dtmaSOH, I_{Fe1}, Fe_2-OOH, and Fe_2-OOH(OH)(μ-O) as the Starting Points[a]

reacn	dtmaSO	dtmaSOH	I_{Fe1}	Fe_2-OOH	Fe_2-OOH(OH)(μ-O)
1a	−18.0	−9.0	−18.3	−13.4	−19.1
2a	−29.1	−26.0	−22.5	−30.3	−37.3
1b	−29.4	−37.3	−37.5	−22.5	−27.3
2b	−17.7	2.3	dissoc	−21.3	−29.1
3a	−12.1	−24.2	−18.4	−15.5	−2.7
$3b^{ext}$	−95.7	−100.7	−104.1	−95.4	−86.5
1c	−34.1	−26.9	−36.2	−30.3	−34.2
4	−16.5	−15.4	−27.7	−26.1	−29.1
5a	−18.2	−26.4	−4.8	−12.3	−5.4
$5b^{ext}$	−121.0	−108.2	−87.5	−85.7	−85.6

[a] Structures were optimized with BP86/RI/TZVP/COSMO ($\varepsilon = 4$) for the total charge of 3−/4− elementary charges, as indicated in Figure 11. Protonation energies were calculated by assuming, for a solvated proton, an energy of −262.4 kcal/mol.[39,40]

aggressive way than molecular oxygen. Judging on the basis of reaction energies, there is no preferred site of H_2O_2 attack on the active site. However, the dtma bridge and Cys_{503} are located in the closest distance to the assumed H_2O_2 formation site and thus are the easiest to reach.

Note, however, that selectivity of H_2O_2-induced oxidation of nucleophilic cysteines was reported by Weerapana et al.[44] Kim et al. proposed an experimental technique to identify those Cys residues that are prone to oxidation by H_2O_2,[45] which could be used to validate our findings experimentally. Interestingly, when we tried to oxidize protonated Cys_{299}, H_2O_2 did not bind to this residue. Hence, not all cysteines have the same sensitivity to H_2O_2. The cysteine residues ligating the iron−sulfur cubane belong to the group which is more readily oxidized. Thus, sulfoxidation is an important, if not the key, factor of O_2 tolerance of hydrogenase enzymes and attack of hydrogen peroxide at the bridging cysteine Cys_{503} might be the first step for the oxidative decomposition of the [FeFe] hydrogenase H cluster.

5. DO PARTIALLY DESTROYED H CLUSTERS SUPPORT THE CATALYTIC PRODUCTION OF ROS?

After having shown possible pathways for the decomposition of the H cluster, an important question remains to be answered: can a partially decomposed H cluster support the production of ROS so that the decomposition process is maintained?

The feasibility of catalytic formation of ROS at partially destroyed H clusters was investigated for the reaction products of H_2O_2 addition to the $2[Fe]_H$ subsite (**dtmaSO** and **dtmaSOH** structures presented in Figure 7c,d) and to Cys_{503} coordinating $[Fe_4S_4]$ cubane (structure $\mathbf{I_{Fe1}}$ depicted in Figure 8a). From OOH-derived degradation products we consider these structures: **Fe_2-OOH** and **Fe_2-OOH(OH)(μ-O)** of Figure 6b,c. The results obtained are summarized in Figure 11 and in Table 2. It turned out that the catalytic formation of ROS remains feasible for all of the considered clusters.

ROS can still be formed at the H cluster even when there are changes in structure of the $2[Fe]_H$ subsite. In the worst case one path of the small cycle (O_2^- release) is energetically not likely to be feasible. For instance, for $\mathbf{I_{Fe1}}$-derived clusters coordination of molecular oxygen must take place before one-electron reduction, because O_2 does not coordinate to the reduced form of $\mathbf{I_{Fe1}}$ due to changes in the position of ligands at the distal iron atom (in the reduced 4− form of $\mathbf{I_{Fe1}}$, the CO ligand moves from a bridging to a terminal position and blocks the free coordination site on Fe_d; O_2 does not bind in a bridging position between Fe_d and Fe_p). Note, however, that due to interactions with, for example, a conserved lysine residue in the protein environment the ligands are not likely to move so that the catalytic activity of the H cluster should be preserved when the whole protein is considered.

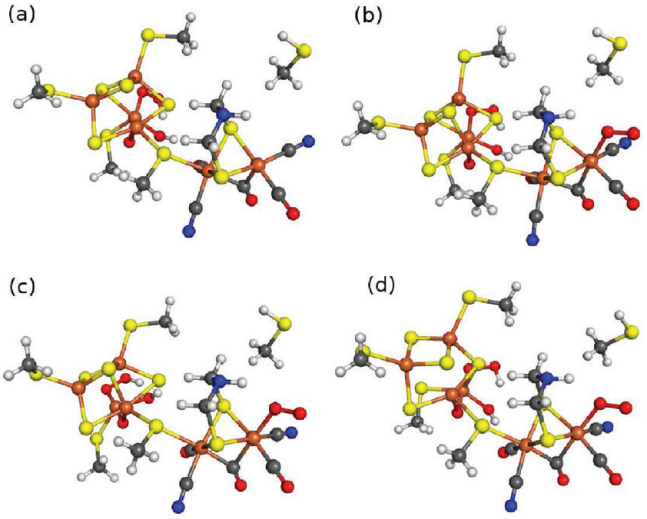

Figure 12. Structures of reaction products of **Fe_2-OOH(OH)(μ-O)**-based ROS formation reaction cycle, optimized with BP86/RI/TZVP/COSMO: (a) **Fe_2-OOH(OH)(μ-O)** (b) **O_2-Fe_2-OOH(OH)(μ-O)** with O_2 coordinated to the distal iron atom Fe_d of **Fe_2-OOH(OH)-(μ-O)**; (c, d) two alternative structures of reduced **O_2-Fe_2-OOH(OH)-(μ-O)** (4− elementary charges) optimized for two different spin coupling schemes of the iron atoms.

Reactions of O_2 at the $2[Fe]_H$ subsite of a partially destroyed H cluster can support further destruction of the cubane structure. For instance, for **Fe_2-OOH(OH)(μ-O)** a coordination of O_2 to the Fe_d atom (−19.1 kcal/mol) and subsequent one-electron reduction (−37.3 kcal/mol) triggers the breaking of one of the bonds between iron and sulfur atoms of the cubane, leaving an iron atom considerably more outside of the cubane structure (see Figure 12).

We should, however, note that for products of OOH-driven degradation the energetics of ROS generation is highly affected by the coupling scheme of the spins at the iron atoms of the cubane (see details given in the Supporting Information).

6. GENERAL IMPLICATIONS FOR OXIDATION OF IRON−SULFUR CLUSTERS IN PROTEINS

The reaction cycle for the formation of ROS described here agrees well with experimental results.[29,22] On the basis of spectroscopic measurements performed on [FeFe] hydrogenase isolated from *C. reinhardtii*, they proposed that enzyme deactivation takes place by the initial reversible formation of an O_2 adduct followed by production of ROS and irreversible modification of the $[Fe_4S_4]$ cubane. Our work provides mechanistic insight into the formation of ROS at the H cluster and discusses possible reaction events that lead to the irreversible changes at the iron−sulfur cubane. We found that $OOH^\bullet$ and H_2O_2 are the most

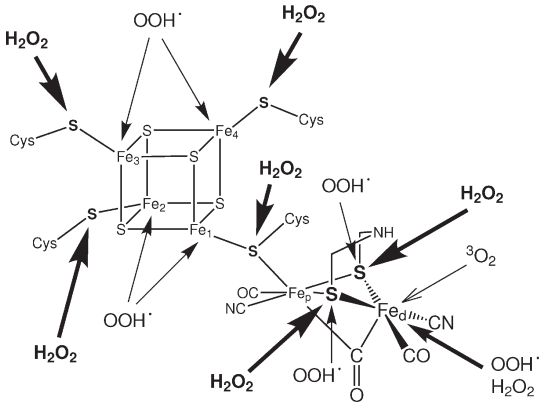

Figure 13. Overview of possible centers of ROS attack. Arrows indicate ROS binding sites. Their thickness qualitatively correlates with the energy released.

probable damaging agents and identified their preferable coordination sites. This part of the results is summarized in Figure 13. The picture of dioxygen-induced inhibition of the H cluster emerging from considerations presented here is complementary to the aforementioned earlier work by us,[23] where the decomposition of the first ligand sphere of the Fe_d atom was proposed. In both studies we investigated double protonation of oxygen adduct **2** (see Figure 2). However, in the first paper protonation of the distal oxygen atom and water release is considered with Fe_d═O being a stable intermediate. In the present work, we focus on the possibility that a second proton is transferred to the oxygen atom proximal to the Fe_d atom and subsequent release of H_2O_2 takes place. Interestingly, the same alternative Fe═O versus H_2O_2 formation was studied for oxidation of the active site of cytochrome P450 by Thiel and coworkers.[46] Their QM/MM study showed that preferred choice of the accepting oxygen atom for the transfer of a second proton depends on the amino acids surrounding the active site. Therefore, it is the logical next step to investigate the influence of the protein environment of the H cluster on the two alternative reaction pathways proposed by our group. These investigations can now be carried out after having established a clear picture of the principles of oxygen inhibition at the generic H cluster.

It is also instructive to compare the degradation pathway proposed here with studies on the decomposition of $[Fe_4S_4]$ cubanes upon oxygen exposure in other enzymes such as aconitase or ferredoxins.[47−49] The main difference between the aconitase iron−sulfur cluster and the $[Fe_4S_4]$ cubane in [FeFe] hydrogenase is in the number of coordinating cysteine residues. For aconitase, one of the iron atoms of the cubane plays a role at the active center and is not coordinated by cysteine. Our calculation shows that coordination of dioxygen to a free iron atom of the $[Fe_4S_4]$ cubane would be energetically favored by more than −15 kcal/mol. Therefore, the decomposition mechanism of the $[Fe_4S_4]$ cubane in aconitase follows most probably a different path, where oxygen can be reduced at the cubane. This is in line with the fact that the final product of oxidation of the $[Fe_4S_4]$ cubane in aconitase is a $[Fe_3S_4]$ cuboidal structure where one Fe atom is removed, most probably in a Fenton reaction (see ref 50 and references therein), while for [FeFe] hydrogenase the final product has not yet been experimentally identified. Another important difference is that aconitase interaction with dioxygen is subsite specific and reversible through $[Fe_3S_4]/[Fe_4S_4]$ cluster interconversion,[50] whereas for [FeFe] hydrogenases dioxygen-induced inhibition is irreversible.

Table 3. Collection of BP86/RI/TZVP Reaction Energies (in kcal/mol) for OOH• Coordinated to an Iron Atom in Fe_2-OOH (Middle Column) and for H_2O_2 Reacted with a Sulfur Atom in I_{Fe2} (Right Column), Respectively[a]

reacn	OOH•	H_2O_2
A	−20.2	−42.4
B	−51.5	−59.8
C	−21.5	−66.8

[a] Reaction A implies addition of the first ROS molecule, reaction B considers addition of a second molecule, and reaction C finally considers addition of a third molecule. Note that the coordination of the first two OOH• radicals is to Fe_2, while the third one is to Fe_4—in accordance with the discussion in the text.

Because of greater structural similarities between hydrogenase and ferredoxins (the iron−sulfur cubane is coordinated by four cysteine ligands in both proteins), the oxygen sensitivity of ferredoxins is easier to compare. No details are known about a possible decomposition pathway, but it is assumed by analogy to aconitase that the degradation of the $[Fe_4S_4]$ cluster should proceed through a $[Fe_3S_4]$ intermediate. However, no spectroscopic evidence for formation of $[Fe_3S_4]$ was found.[51]

A very recently studied example of an O_2-sensitive protein containing a $[Fe_4S_4]$ cluster is the transcriptional regulator FNR.[48,49,52] A crystal structure of this protein has not yet been solved, and the discussion in the literature is based on a homology model. The distance between Cys_{122} and the cubane is proposed to be longer than for three other ligating residues. However, in the work of Jervis et al.[49] the site of Cys_{23} at the cubane is considered to be the primary site of dioxygen attack. Jervis et al. show that shielding an iron−sulfur bond between the Cys_{23} and an iron atom from the cubane can slow down destructive O_2 interaction. ROS attack at an iron−sulfur bond in one of the cysteine residues ligating the cubane is in line with the findings of this study.

7. CONCLUSIONS

In this work we have studied the O_2-induced deactivation of the H cluster by uncovering the formation of reactive oxygen species at this active site and subsequent attack of the cubane structure. The most important findings of this study are summarized as follows.

1. Triplet dioxygen does not bind to the cubane subsite of the H cluster. We find, however, that catalytic formation of ROS (O_2^- and OOH^-) at Fe_d is feasible—even after parts of the H cluster have already been degraded—and consider it an intrinsic pathological property of the H cluster. At the same time these results explain the protection of the enzyme by the reversible inhibitor CO.[29]
2. For the inactive oxidized form H_{ox}^{inact} the formation of ROS is energetically not feasible. This explains the experimentally observed O_2 tolerance of the cluster in this state.[2]
3. O_2^- and OOH^- are not likely to directly act as damaging agents, but we find that OOH• and H_2O_2 can be formed in close proximity to the $[Fe_4S_4]$ cubane by protonation of O_2^- and OOH^-, respectively. It is shown that OOH• and H_2O_2 are able to oxidize the iron−sulfur cubane, most likely leading to its experimentally observed[29] decomposition.

4. We identify the primary site of H_2O_2 attack to be the cysteine ligands coordinating the $[Fe_4S_4]$ unit, which is in contrast to $OOH^•$, which shows preferable binding directly to the iron atoms of the H cluster (see Figure 13). Therefore, it should be possible to detect sulfoxides in the oxygen-inhibited form of [FeFe] hydrogenase when H_2O_2 is the oxidizing agent. Oxidation of sulfur atoms of the dtma ligand is also energetically feasible; however, it does not lead to any major changes in the structure of the H cluster.

For the sake of convenience, we collect the reaction energies obtained for the attack of up to three $OOH^•$ and H_2O_2 molecules, respectively, to a selected structure of the H cluster in Table 3. Despite many years of intense research on the decomposition of iron−sulfur cubanes upon dioxygen exposure, no detailed mechanism for the oxidation has yet been established. We find pronounced structural changes in the $[Fe_4S_4]$ cubane induced by ROS. The results obtained here for the H cluster might not only apply to hydrogenases but could be generalized to other enzymes harboring iron−sulfur cubanes such as aconitase and ferredoxins. In order to investigate such a generalization, work on these enzymes has been initiated in our laboratory.

This work on the isolated H cluster forms the basis for understanding the influence of the protein structure on cluster reactivity toward oxygen inhibition which we will study in our laboratory for a large QM model of the active site that allows us to consider amino acid exchanges in the vicinity of the H cluster.

A. APPENDIX: COMPUTATIONAL METHODOLOGY

Because of the very delicate electronic structure of the H cluster, the computational methodology applied requires more precautions than usual, as shall be discussed in this Appendix.

A.1. General Setup Structure optimizations have been carried out using the density functional programs provided by the Turbomole 5.10 suite.[53] Atomic coordinates of the starting structures of the oxygen-free models of the active site were obtained from the X-ray structure of the H cluster from *Clostridium pasteurianum* [FeFe] hydrogenase.[33] One hydrogen atom, saturating the broken bonds to the protein scaffold, and the carbon atom it binds to were kept fixed along the $C_\alpha-C_\beta$ bond in the protein in all structure optimizations. This anchoring of the H cluster ensures a spatial fixation that resembles the fixation in the protein's active site and ensures that the directional character of the anchoring amino acids is preserved as well.

All results were obtained from unrestricted, all-electron Kohn−Sham calculations employing the Becke−Perdew functional BP86[54,55] with the resolution of the identity (RI) density fitting approximation. This functional was chosen because it yields reliable structures and reaction energetics for models of the active sites of [FeFe] hydrogenase.[7,23,27,56,57] For selected structures we have also performed calculations with the B3LYP[58,59] hybrid functionals in order to probe the sensitivity of our results with respect to the density functional chosen. For all atoms Ahlrichs' valence triple-ζ def-TZVP basis set with polarization functions was used.[60] All molecular structures were fully optimized for the spin states considered, applying tight convergence thresholds (the orbitals were converged until the electronic energy was constant up to the seventh decimal place, and structures were optimized until the length of the geometry gradient dropped below a value of 10^{-4} atomic units). The basis set superposition error of the TZVP basis set with respect to coordination energies was estimated to be about 2.4 kcal/mol[61] and should therefore not affect our conclusions. The vibrational analysis for the transition state search has been carried out with the SNF program package.[62]

All reaction energies presented in the paper have been evaluated at 0 K without vibrational and temperature corrections. The reason for this choice is the fact that enthalpy differences are often very similar to electronic energy differences (the deviation between both differences is usually smaller than the accuracy one may expect for DFT calculations on transition-metal clusters) and Gibbs free enthalpy differences calculated for the gas phase deviate from condensed-phase free enthalpy differences by about 15 kcal/mol in reactions that involve numbers of molecules on the educt and product sides that deviate by 1 (because translational entropy contributions are not properly balanced in the standard gas-phase harmonic-oscillator rigid-rotor particle in a box approximation when directly compared to the condensed phase[61]). Reduction reactions of the cluster structures were calculated as the transfer of a free electron with zero kinetic energy; i.e., they are obtained by subtraction of electronic energies for the original species from its optimized reduced counterpart. As a consequence, the reduction energies are intrinsic reduction energies of the cluster structures that do not take the ionization energy of a reductant into account. The program PyMOL[63] was used for the visualization of structures.

A.2. Spin Coupling. Different possible ferromagnetic and antiferromagnetic coupling patterns of the iron atoms of the H cluster were considered within the broken symmetry (BS) approach.[64−67] While we initially used our restrained optimization scheme[68] to converge specific coupling patterns, we found that the various possible BS solutions can be more easily created following the strategy suggested by Greco et al.[69] This means that for each structure a single-point open-shell self-consistent-field calculation at low-spin multiplicity was performed in order to obtain one of the possible BS solutions. For the converged molecular orbitals a population analysis was performed in order to identify the antiferromagnetically coupled iron atoms identified by opposite signs of local $\langle S_{zA}\rangle$ expectation values.[70−72] For this, we used our local version of the Moloch module of Turbomole 5.1.[70,71] Then, alternative BS solutions were generated by optimizing the given set of molecular orbitals for exchanged coordinates of pairs of iron atoms featuring spin populations with opposite signs as proposed by Greco et al.[69] These BS determinants are then used for the optimization of the molecular structures. It is important to note that the choice of the BS coupling pattern determines the molecular structure obtained by optimization. We made every possible effort not to overlook any of the possible structures and carried out numerous optimizations, of which we report only the final results for the lowest-energy BS solutions. Finally, we should refer the reader to the Supporting Information, where we compiled more details on the broken-symmetry calculations and how they might affect the results.

A.3. Modeling of Solvation. Since we consider reactions between species with various electrical charges and processes involving charge separations, we applied the continuum solvation model COSMO,[34] as implemented in Turbomole, in order to account for the effect of charge stabilization by the protein environment. Unless otherwise stated, the discussion is based on the results of structure optimizations obtained by considering a COSMO representation to model a dielectric environment with a dielectric constant of $\varepsilon = 4$.[27] It must be noted that

molecular structure optimizations with and without COSMO may yield different results. Therefore, we would optimize structures obtained in an isolated-molecule optimization also in a COSMO environment, if both structures had turned out to be qualitatively different.

We should emphasize that the reaction energies for addition of ROS to the active site of [FeFe] hydrogenases are difficult to describe accurately using DFT, especially for processes involving proton transfer. Despite the employed COSMO solvation model, the highly exothermic energy for the transfer of (solvated) protons is obviously due to charge recombination at the negatively charged cluster. Therefore, considering the energetics of internal proton transfer from Cys_{299}, a residue often considered as a possible proton donor during the catalytic cycle of [FeFe] hydrogenase,[73] is more reliable than adding an external proton to a cluster structure. However, it is important to note that it turned out to not affect the conclusions that we have been able to draw from the calculated results.

In general, protonation energies were calculated by assuming an energy of −262.4 kcal/mol for a (external) solvated proton.[39,40] Protonation of the distal oxygen adduct **2** in the reduced state (4− elementary charges) from Eigen and Zundel ions[74] was also investigated. The charge recombination is still the major problem when protonation from such water clusters is considered, and unless the whole proton transfer chain is modeled, it can hardly be avoided. The energy of protonation with the "solvated-proton" model is equal to −100.6 kcal/mol, for protonation from an Eigen ion it is −142.9 kcal/mol, and from a Zundel ion it is −127.6 kcal/mol. The solvated-proton model, employed consistently throughout this paper, may be considered to provide an upper bound to the exothermic energy of a proton transfer from a water cluster, and therefore, it is a satisfactory solution.

A.4. Comparison to Coupled-Cluster Results for Model Reactions. In order to assess the reliability of the DFT functionals employed in this work, it is important to compare with reference ab initio results. However, these are hard to obtain and we made an attempt to compare to single-reference coupled-cluster data that we calculated with the Molpro 2009.1 package.[75] Coupled-cluster benchmark calculations of reaction energies are feasible only for small molecules. We therefore decided to consider very small model reactants and chose reactions 1−3 in accordance with those studied in this paper for the large cluster models for which coupled-cluster calculations are neither feasible nor suitable. Note that a reaction similar to eq 3 but with H_2S instead of FeH_2 does not produce the product $H_2SOOH^{\bullet}$, as $HOO^{\bullet}$ does not bind to H_2S (BP86/RI/TZVP). In reaction 2, the product HFe(O)OH features a broken O−O bond (the molecule HFeOOH is not stable upon structure optimization).

$$H_2O_2 + H_2S \rightarrow H_2 + HSOOH \quad (1)$$

$$H_2O_2 + FeH_2 \rightarrow H_2 + HFe(O)OH \quad (2)$$

$$HOO^{\bullet} + FeH_2 \rightarrow H_2FeOOH^{\bullet} \quad (3)$$

Structures of the small model molecules involved in the reactions have been optimized with BP86/RI/TZVP, and all subsequent energy calculations were performed as single points on these structures employing DFT with the pure BP86 and TPSS,[76] the hybrid B3LYP, and the double-hybrid B2PLYP[77] exchange−correlation functionals as well as with the wave function based methods Møller−Plesset perturbation theory to second order (MP2) and coupled cluster singles and doubles plus perturbatively treated triples excitations (CCSD(T))[78] (with Dunning's correlation-consistent aug-cc-pVDZ and aug-cc-pVTZ basis sets[79−81]) . The results reported in Table 4 allow us to assess the accuracy of the DFT results applied in this work.

Table 4. Comparison of Reaction Energies (kcal/mol) Obtained for Reactions 1−3[a]

	reacn		
	1	2	3
BP86/def-TZVP	40.6	−126.3	−98.3
B3LYP/def-TZVP	42.2	−98.6	−75.6
B2PLYP/def-TZVP	42.3	−130.6	−76.6
TPSS/def-TZVP	37.4	−122.8	−94.0
MP2/aug-cc-pVDZ	44.7	−145.9	−70.8
SCS-MP2/aug-cc-pVDZ	44.0	−124.6	
CCSD/aug-cc-pVDZ	46.0	−83.8	−61.2
CCSD(T)/aug-cc-pVDZ	44.1	−109.0	−74.4
MP2/aug-cc-pVTZ	42.2	−147.5	−78.6
SCS-MP2/aug-cc-pVTZ	41.5	−125.6	
CCSD/aug-cc-pVTZ	44.1	−82.9	−64.5
CCSD(T)/aug-cc-pVTZ	42.1	−109.3	−76.6

[a] The energies were obtained for single-point calculations on BP86/RI/TZVP-optimized structures. As correlation methods such as MP2 and CCSD(T) may strongly depend on the basis set, we report results for aug-cc-pVDZ and aug-cc-pVTZ basis sets.

The CCSD(T)/aug-cc-pVTZ results may be considered as the most accurate results. However, as it is not clear whether the single-reference methods MP2, CCSD, and CCSD(T), which are all based on a single Hartree−Fock reference determinant, can be applied to the transition-metal model complexes, we may report the T1 diagnostic as an indicator for their applicability: it was about 0.09 for all iron compounds. Since spin-component-scaled MP2 (SCS-MP2)[82] is generally believed to improve on MP2 in critical cases, we also report such results in Table 4.

For reaction 1 involving only main-group elements the DFT results are very similar to the CCSD(T)/aug-cc-pVTZ reference, indicating that this might also hold for our ROS reactions with sulfur atoms in our H cluster models. All approaches deliver similar reaction energies within a range of about 4 kcal/mol. For reactions 2 and 3 involving an iron atom, the differences in reaction energies are more pronounced. Out of the density functionals employed, the best agreement with the CCSD(T)/aug-cc-pVTZ data is obtained for B3LYP. However, considering the fact that model reactions are studied, this better agreement of B3LYP must not be overrated, but this finding prompted us to include B3LYP results in Table 1 for a direct comparison to the BP86 reaction energies.

Not unexpectedly, the double hybrid B2PLYP with its second-order perturbation correction to describe electron correlation yields results similar to those for MP2 and may overestimate reaction energies by about 40% (see the results for reaction 2 in Table 4). The BP86 functional overestimates the reaction energy for reaction 2 by about 20 kcal/mol in comparison with CCSD(T)/aug-cc-pVTZ. For reaction 3 BP86 and TPSS (both non-hybrid functionals) overbind compared to CCSD(T) (21.7 kcal/mol more exothermic than CCSD(T)/aug-cc-pVTZ). As can be seen from Table 4 by comparing CCSD(T) and CCSD results for reactions 2 and 3, the inclusion of triple excitations for

reactions involving iron is very important. The differences in reaction energies between CCSD and CCSD(T) can be more than 20 kcal/mol (reaction 2). Interestingly, the small aug-cc-pVDZ basis set yields energies within about 3 kcal/mol of the aug-cc-pVTZ results.

As a conclusion from these benchmark calculations, we see that the DFT results are qualitatively always correct, they are quantitative for reactions that involve main-group elements (ROS attack at sulfur atoms) and better than semiquantitative for those that involve iron atoms. Also, one must keep in mind that a single-reference coupled cluster may not be without flaws for unsaturated transition-metal compounds and has to be considered with care as a reference method. Hence, the reaction energies reported in this paper may be considered to be better than semiquantitative. Moreover, for the discussion in this paper it must be emphasized that our DFT calculations on H cluster models yield not only energies but also, most importantly, structural information, which allows us to identify possible stable intermediates. Moreover, we should note that our quantum chemical study is complementary to the multiscale modeling method for the calculation of gas diffusion rates inside proteins recently presented by Blumberger and co-worker.[83,84] Their approach revealed multiple ways of transport of gas molecules into the active site of [NiFe] hydrogenase, which can be taken as a justification for our investigation of structures that allow ROS to access the active site from any direction.

■ ASSOCIATED CONTENT

Supporting Information. Text, figures, and tables giving a detailed discussion of the relevance of different spin coupling schemes, absolute (electronic) energies, and the coordinates of the atoms in all the molecules whose geometries were optimized. This material is available free of charge via the Internet at http://pubs.acs.org.

■ AUTHOR INFORMATION

Corresponding Author
*E-mail: markus.reiher@phys.chem.ethz.ch.

■ ACKNOWLEDGMENT

This work was financially supported by the Swiss National Science Foundation (Project No. 200020-132542/1).

■ REFERENCES

(1) Vignais, P. M.; Billoud, B.; Meyer, J. *FEMS Microbiol. Rev.* **2001**, *25*, 455–501.
(2) Vincent, K. A.; Parkin, A.; Armstrong, F. A. *Chem. Rev.* **2007**, *107*, 4366–4413.
(3) Lubitz, W.; Reijerse, E.; van Gastel, M. *Chem. Rev.* **2007**, *107*, 4331–4365.
(4) Siegbahn, P. E. M.; Tye, J. W.; Hall, M. B. *Chem. Rev.* **2007**, *107*, 4414–4435.
(5) Greco, C.; Bruschi, M.; De Gioia, L.; Ryde, U. *Inorg. Chem.* **2007**, *46*, 5911–5921.
(6) Heinekey, D. M. *J. Organomet. Chem.* **2009**, *694*, 2671–2680.
(7) Bruschi, M.; Greco, C.; Kaukonen, M.; Fantucci, P.; Ryde, U.; Gioia, L. D. *Angew. Chem., Int. Ed.* **2009**, *48*, 3503–3506.
(8) Cracknell, J. A.; Vincent, K. A.; Ludwig, M.; Lenz, O.; Friedrich, B.; Armstrong, F. A. *J. Am. Chem. Soc.* **2008**, *130*, 424–425.
(9) Lubner, C. E.; Knörzer, P.; Silva, P. J. N.; Vincent, K. A.; Happe, T.; Bryant, D. A.; Golbeck, J. H. *Biochemistry* **2010**, *49*, 10264–10266.
(10) Friedrich, B.; Fritsch, J.; Lenz, O. *Curr. Opin. Biotechnol.* **2011**, *23*, 358–364.
(11) Shima, S.; Thauer, R. K. *Chem. Rev.* **2007**, *7*, 37–46.
(12) Yang, X.; Hall, M. B. *J. Am. Chem. Soc.* **2009**, *131*, 10901–10908.
(13) Volbeda, A.; Martin, L.; Cavazza, C.; Matho, M.; Faber, B. W.; Roseboom, W.; Albracht, S. P. J.; Garcin, E.; Rousset, M.; Fontecilla-Camps, J. C. *J. Biol. Inorg. Chem.* **2005**, *10*, 239–249.
(14) Dementin, S.; Lerouxi, F.; Cournac, L.; de Lacey, A. L.; Volbeda, A.; Léger, C.; Burlat, B.; Martinez, N.; Champ, S.; Martin, L.; Sanganas, O.; Haumann, M.; Fernández, V. M.; Guigliarelli, B.; Fontecilla-Camps, J. C.; Rousset, M. *J. Am. Chem. Soc.* **2009**, *131*, 10156–10164.
(15) Liebgott, P.-P.; Leroux, F.; Burlat, B.; Dementin, S.; Baffert, C.; Lautier, T.; Fourmond, V.; Ceccaldi, P.; Cavazza, C.; Meynial-Salles, I.; Soucaille, P.; Fontecilla-Camps, J. C.; Guigliarelli, B.; Bertrand, P.; Rousset, M.; Léger, C. *Nat. Chem. Biol.* **2010**, *6*, 63–70.
(16) Ludwig, M.; Cracknell, J. A.; Vincent, K. A.; Armstrong, F. A.; Lenz, O. *J. Biol. Chem.* **2009**, *284*, 465–477.
(17) Löscher, S.; Gebler, A.; Stein, M.; Sanganas, O.; Buhrke, T.; Zebger, I.; Dau, H.; Friedrich, B.; Lenz, O.; Haumann, M. *ChemPhysChem* **2010**, *11*, 1297–1306.
(18) Goris, T.; Wait, A. F.; Saggu, M.; Fritsch, J.; Heidary, N.; Stein, M.; Zebger, I.; Lendzian, F.; Armstrong, F. A.; Friedrich, B.; Lenz, O. *Nat. Chem. Biol.* **2011**, *7*, 310–318.
(19) Pandelia, M.-E.; Ogata, H.; Lubitz, W. *ChemPhysChem* **2010**, *11*, 1127–1140.
(20) Adams, M. W. W. *Biochim. Biophys. Acta* **1990**, *1020*, 115.
(21) Fontecilla-Camps, J. C.; Volbeda, A.; Cavazza, C.; Nicolet, Y. *Chem. Rev.* **2007**, *107*, 4273–4303.
(22) Baffert, C.; Demuez, M.; Cournac, L.; Burlat, B.; Guigliarelli, B.; Bertrand, P.; Girbal, L.; Léger, C. *Angew. Chem., Int. Ed.* **2008**, *47*, 2052–2054.
(23) Stiebritz, M. T.; Reiher, M. *Inorg. Chem.* **2009**, *48*, 7127–7140.
(24) Dogaru, D.; Motiu, S.; Gogonea, V. *Int. J. Quantum Chem.* **2009**, *109*, 876–889.
(25) Stiebritz, M. T.; Reiher, M. *Inorg. Chem.* **2010**, *49*, 5818–5823.
(26) Stiebritz, M. T.; Bruska, M. K.; Reiher, M. Data presented at the 9th International Hydrogenase Conference in Uppsala, Sweden; June 2010.
(27) Stiebritz, M. T.; Finkelmann, A. R.; Reiher, M. *Eur. J. Inorg. Chem.* **2011**, 1163–1171.
(28) Dey, A. *J. Am. Chem. Soc.* **2010**, *132*, 13892–13901.
(29) Stripp, S. T.; Goldet, G.; Brandmayr, C.; Sanganas, O.; Vincent, K. A.; Haumann, M.; Armstrong, F. A.; Happe, T. *Proc. Natl. Acad. Sci. U.S.A.* **2009**, *106*, 17331–17336.
(30) Flint, D. H.; Tuminello, J. F.; Emptage, M. H. *J. Biol. Chem.* **1993**, *268*, 22369–22376.
(31) Darensbourg, M. Y.; Weigand, W. *Eur. J. Inorg. Chem.* **2011**, 994–1004.
(32) Stiebritz, M. T.; Reiher, M. *Inorg. Chem.* **2010**, *49*, 8645.
(33) Pandey, A. S.; Harris, T. V.; Giles, L. J.; Peters, J. W.; Szilagyi, R. K. *J. Am. Chem. Soc.* **2008**, *130*, 4533–4540.
(34) Klamt, A.; Jonas, V. *J. Chem. Phys.* **1996**, *105*, 9972–9981.
(35) Mulder, D. W.; Boyd, E. S.; Sarma, R.; Lange, R. K.; Endrizzi, J. A.; Broderick, J. B.; Peters, J. W. *Nature* **2010**, *465*, 248–251.
(36) Reiher, M.; Salomon, O.; Hess, B. A. *Theor. Chem. Acc.* **2001**, *107*, 48–55.
(37) Reiher, M. *Inorg. Chem.* **2002**, *41*, 6928–6935.
(38) Salomon, O.; Reiher, M.; Hess, B. A. *J. Chem. Phys.* **2002**, *117*, 4729–4737.
(39) Klots, C. E. *J. Phys. Chem.* **1981**, *85*, 3585–3588.
(40) Topol, I. A.; Tawa, G. J.; Burt, S. K.; Rashin, A. A. *J. Phys. Chem.* **1997**, *101*, 10075–10081.
(41) Takahashi, M.; Asada, K. *J. Biochem.* **1982**, *91*, 889–896.
(42) Baffert, C.; Bertini, L.; Lautier, T.; Greco, C.; Sybirna, K.; Ezanno, P.; Etienne, E.; Soucaille, P.; Bertrand, P.; Bottin, H.; Meynial-Salles, I.; Gioia, L. D.; Léger, C. *J. Am. Chem. Soc.* **2011**, *133*, 2096–2099.
(43) Roth, E. K. H.; Jordanov, J. *Inorg. Chem.* **1992**, *31*, 240–243.

(44) Weerapana, E.; Wang, C.; Simon, G. M.; Richter, F.; Khare, S.; Dillon, M. B. D.; Bachovchin, D. A.; Mowen, K.; Baker, D.; Cravatt, B. F. *Nature* **2010**, *468*, 790–795.
(45) Kim, J.-R.; Yoon, H. W.; Kwon, K.-S.; Lee, S.-R.; Rhee, S. G. *Anal. Biochem.* **2000**, *283*, 214–221.
(46) Altarsha, M.; Benighaus, T.; Kumar, D.; Thiel, W. *J. Am. Chem. Soc.* **2009**, *131*, 4755–4763.
(47) Holm, R. H.; Ciurli, S.; Weigel, J. A. *Prog. Inorg. Chem.* **2007**, *38*, 1–74.
(48) Crack, J. C.; Gaskell, A. A.; Green, J.; Cheesman, M. R.; Brun, N. E. L.; Thomson, A. J. *J. Am. Chem. Soc.* **2008**, *130*, 1749–1758.
(49) Jervis, A. J.; Crack, J. C.; White, G.; Artymiuk, P. J.; Cheesman, M. R.; Thomson, A. J.; Brun, N. E. L.; Green, J. *Proc. Natl. Acad. Sci. U.S.A.* **2009**, *106*, 4659–4664.
(50) Holm, R. H.; Kennepohl, P.; Solomon, E. I. *Chem. Rev.* **1996**, *96*, 2239–2314.
(51) Bian, S.; Hemann, C. F.; Hille, R.; Cowan, J. A. *Biochemistry* **1996**, *35*, 14544–14552.
(52) Crack, J. C.; Green, J.; Cheesman, M. R.; Brun, N. E. L.; Thomson, A. J. *Proc. Natl. Acad. Sci. U.S.A.* **2007**, *104*, 2092–2097.
(53) Ahlrichs, R.; Bär, M.; Häser, M.; Horn, H.; Kölmel, C. *Chem. Phys. Lett.* **1989**, *162*, 165–169.
(54) Becke, A. D. *Phys. Rev. A* **1988**, *38*, 3098–3100.
(55) Perdew *Phys. Rev. B* **1986**, *33*, 8822–8824.
(56) Bruschi, M.; Greco, C.; Bertini, L.; Fantucci, P.; Ryde, U.; Gioia, L. D. *J. Am. Chem. Soc.* **2010**, *132*, 4992–4993.
(57) Yu, L.; Greco, C.; Bruschi, M.; Ryde, U.; De Gioia, L.; Reiher, M. *Inorg. Chem.* **2011**, *50*, 3888–3900.
(58) Lee, C.; Yang, W.; Parr, R. G. *Phys. Rev. B* **1988**, *37*, 785–789.
(59) Becke, A. D. *J. Chem. Phys.* **1993**, *98*, 5648–5652.
(60) Schäfer, A.; Huber, C.; Ahlrichs, R. *J. Chem. Phys.* **1994**, *100*, 5829–5835.
(61) Reiher, M.; Hess, B. A. *Chem. Eur. J.* **2002**, *8*, 5332–5339.
(62) Neugebauer, J.; Reiher, M.; Kind, C.; Hess, B. A. *J. Comput. Chem.* **2002**, *23*, 895–910.
(63) DeLano, W. L. *The PyMOL Molecular Graphics System*; DeLano Scientific, San Carlos, CA, 2002.
(64) Noodleman, L.; Norman, J. G. *J. Chem. Phys.* **1979**, *70*, 4903–4906.
(65) Noodleman, L. *J. Chem. Phys.* **1981**, *74*, 5737–5743.
(66) Herrmann, C.; Yu, L.; Reiher, M. *J. Comput. Chem.* **2006**, *27*, 1223–1239.
(67) Podewitz, M.; Reiher, M. *Adv. Inorg. Chem.* **2010**, *62*, 177–230.
(68) Herrmann, C.; Podewitz, M.; Reiher, M. *Int. J. Quantum Chem.* **2009**, *109*, 2430–2446.
(69) Greco, C.; Fantucci, P.; Ryde, U.; de Gioia, L. *Int. J. Quantum Chem.* **2010**, *111*, 3949–3960.
(70) Herrmann, C.; Reiher, M.; Hess, B. A. *J. Chem. Phys.* **2005**, *122*, 034102.
(71) Podewitz, M.; Herrmann, C.; Malassa, A.; Westerhausen, M.; Reiher, M. *Chem. Phys. Lett.* **2008**, *451*, 301–308.
(72) Reiher, M. *Faraday Discuss.* **2007**, *135*, 97–124.
(73) Peters, J. W.; Lanzilotta, W. N.; Lemon, B. J.; Seefeldt, L. C. *Science* **1998**, *282*, 1853–1858.
(74) Kirchner, B. *ChemPhysChem* **2007**, *8*, 4143.
(75) Werner, H.-J.; Knowles, P. J.; Knizia, G.; Manby, F. R.; Schütz, M.; *WIRes: CMS* **2011**, DOI: 10.1002/wcms.82.
(76) Tao, J.; Perdew, J. P.; Staroverov, V. N.; Scuseria, G. E. *Phys. Rev. Lett.* **2003**, *91*, 146401.
(77) Grimme, S. *J. Chem. Phys.* **2005**, *124*, 034108.
(78) Helgaker, T.; Jørgensen, P.; Olsen, J. *Molecular Electronic-Structure Theory*; Wiley: Chichester, U.K., 2000.
(79) Dunning, T. H., Jr. *J. Chem. Phys.* **1989**, *90*, 1007–1023.
(80) Woon, D. E.; Dunning, T. H. *J. Chem. Phys.* **1993**, *98*, 1358−1371.
(81) Balabanov, N. B.; Peterson, K. A. *J. Chem. Phys.* **2005**, *123*, 064107.
(82) Grimme, S. *J. Chem. Phys.* **2003**, *118*, 9095.
(83) Wang, P.; Bese, R. B.; Blumberger, J. *J. Phys. Chem. Chem. Phys.* **2011**, *13*, 7708–7719.
(84) Wang, P.; Bese, R. B.; Blumberger, J. *J. Phys. Chem. Phys.* **2011**, *133*, 3548–3556.